Optimal Multi-Client Trajectory Planning for A Low-Thrust Servicing Satellite in the Presence of Perturbations

The Journal of the Astronautical Sciences (2025) 72:7
https://doi.org/10.1007/s40295-025-00487-6

ORIGINAL ARTICLE

Optimal Multi-Client Trajectory Planning for A Low-Thrust Servicing Satellite in the Presence of Perturbations

Riccardo Apa[1] · **Shambo Bhattacharjee**[2] · **Jennifer Hudson**[2] · **Marcello Romano**[3]

Accepted: 18 February 2025

Abstract

This paper presents a general method to solve space logistics trajectory optimization problems in the case of low-thrust propulsion. The problem of multiple orbital transfers is considered for a servicing satellite that must visit a set of client satellites only once. A near-optimal distance metric based on the Q-law feedback controller is adopted in order to quantify the cost of the transfer of the servicing satellite between each pair of client-satellite orbits. This distance metric is evaluated for a discrete set of departure orbits, arrival orbits, initial servicer masses, i.e., mass before the transfer, and departure times. A four-dimensional array representing the overall cost is then constructed, and its elements are interpolated in order to efficiently solve the tour-optimization problem using genetic algorithms, particle swarm optimization, and simulated annealing. Both minimum-time and minimum-fuel problems are considered. The proposed method accounts for the following time-dependent factors: secular J_2 perturbations, eclipse power constraints, and fuel mass depletion. The proposed method is tested on a case study involving 20 client satellites with low eccentricity and low inclination, between medium Earth orbit and geosynchronous Earth orbit, and with randomly distributed right ascension of the ascending node and argument of perigee. The efficiency and accuracy of the proposed approach are assessed by comparing the results to solutions found by a direct optimization method.

Keywords Astrodynamics · Low-thrust trajectories · Space logistics · Traveling salesman problem

List of Symbols

$a \in \mathbb{R}^+$	Semi-major axis [m]
$\alpha \in [-180, 180]$	In-plane control thrust angle [deg] – Angle between the projection of the thrust vector onto the RT plane and the transverse (T) direction. Positive when the radial component of the thrust vector is positive.

Extended author information available on the last page of the article

Published online: 11 March 2025

$\beta \in [-90, 90]$	Out-of-plane control thrust angle [deg] - Angle between the thrust vector and its projection onto the RT plane. Positive when the normal component of the thrust vector is positive.
$C \in \mathbb{R}$	Distance metric
$\mathcal{D}$	Set of satellites IDs
Δ	Finite differential operator
$\Delta V \in \mathbb{R}^+$	Velocity increment [m/s]
$e \in [0, 1]$	Eccentricity [-]
$f_{\Delta V}$	Velocity increment bilinear interpolation function
f_{ToF}	Time of flight bilinear interpolation function
$i \in [0, 180]$	Inclination [deg]
$I_{sp} \in \mathbb{R}^+$	Specific impulse [s]
$J_2 \in \mathbb{R}^+$	Second zonal harmonic coefficient [-]
$m_i \in \mathbb{R}^+$	Initial mass [kg]
$\mu \in \mathbb{R}^+$	Earth gravitational parameter [m^3/s^2]
$m_0 \in \mathbb{R}^+$	Total mass [kg]
$m_{dry} \in \mathbb{R}^+$	Dry mass [kg]
$\overline{d} \in \mathbb{N}$	Problem initial orbit ID [-]
$N_{gen} \in \mathbb{N}$	Number of generations [-]
$N_M \in \mathbb{N}$	Number of initial mass discretization points [-]
$N_d \in \mathbb{N}$	Subset dataset size [-]
$N_{pop} \in \mathbb{N}$	Population size [-]
$N_{run} \in \mathbb{N}$	Number of runs [-]
$N_{sat} \in \mathbb{N}$	Number of satellites [-]
$N_{stall} \in \mathbb{N}$	Number of stall generation [-]
$N_T \in \mathbb{N}$	Number of departure time discretization points [-]
$\omega \in [0, 360]$	Argument of perigee [deg]
$\Omega \in [0, 360]$	Right Ascension of the Ascending Node [deg]
$\mathbf{p}$	Distance metric parameters
$R_e \in \mathbb{R}^+$	Earth mean radius [m]
$ToF \in \mathbb{R}^+$	Time of flight [s]
$t_f \in \mathbb{R}^+$	Arrival time [s]
$t_i \in \mathbb{R}^+$	Departure time [s]
$t \in \mathbb{R}^+$	Time [s]
$\mathbf{T} \in \mathbb{R}^3$	Control thrust law described in the radial, transverse, and out-of-plane (RTN) frame [N]
$\mathcal{T}$	Set of control thrust functions
$T_{max} \in \mathbb{R}^+$	Maximum available thrust [N]
$t_0 \in \mathbb{R}^+$	Mission start time [s]
$\mathbf{ToF} \in \mathbb{R}^{+N_d}$	Times of flight [s]
$\mathbf{X}$	State of the satellite
$\theta \in [0, 360]$	True anomaly [deg]
$V \in \mathbb{R}^+$	Orbital velocity magnitude [m/s]
$w_{ecl} \in [0, 1]$	Eclipse factor [-]
$z \in \mathbb{N}$	Number of distance metric evaluations [-]

$\mathbf{Z}_{eq}$	Equality constraints
$\mathbf{Z}_{ineq}$	Inequality constraints

Subscripts

err	Error value
min	Minimum value
max	Maximum value
opt	Optimal value
tot	Total sequence value

1 Introduction

In-space servicing and on-orbit fuel depot positioning are among the most interesting application areas for space logistics [1, 2]. Many of these missions fall into the category of multiple-visitation problems, requiring multiple rendezvous between a servicer spacecraft and multiple client spacecraft. As the propellant of the spacecraft is limited, tour optimization becomes necessary.

Satellite motion is governed by orbital dynamics and affected by various perturbations; therefore, any space-based tour optimization problem involving rendezvous belongs to the class of *"Moving-Target (or time-dependent) Path Optimization Problems"* (MTPOPs). These problems are Nondeterministic Polynomial-time complete (NP-complete) [3] and become very complicated when a large number of clients is considered ($N_{sat} \gtrsim 5$).

The overall problem can be reduced to a time-dependent nonlinear problem, consisting of the following two subproblems [4]:

1. **Functional subproblem:** The cost of each orbital transfer maneuver (*distance metric*) is computed by solving an optimal control problem.
2. **Combinatorial subproblem:** The optimal sequence of clients is selected to minimize the overall cost.

Even considered separately, these two subproblems are hard to solve. Previously, several authors [5–9] suggested using a servicer equipped with a high-thrust propulsion system. This assumption simplifies the functional problem, as it limits the number of variables. Additionally, these studies used distance metrics based on either non-optimal control theory [7] or predefined sequences of impulsive maneuvers to quantify the cost associated with each maneuver [5–8]. Also, most previous works have not considered the effect of perturbations, such as accelerations induced by higher-order harmonics of the geopotential and atmospheric drag. Due to the presence of various perturbations, the cost of maneuvering from orbit i to j becomes different from the cost of maneuvering from j to i.

Regardless of the effect of perturbations, the main disadvantage of using high-thrust propulsion for multiple rendezvous is that the fuel requirements become

enormous even for visiting a very small number of clients. To overcome this issue, Cerf [8] includes passive Right Ascension of the Ascending Node (RAAN) correction, by exploiting a drift orbit to reduce fuel consumption.

The use of low-thrust propulsion is proposed in literature as an alternative strategy to serve a larger number of satellites [10–16]. Due to the complexity of the problem, these studies adopt assumptions regarding the functional problem and/or the combinatorial one to obtain a solution.

Hudson and Kolosa [10] address an on-orbit servicing mission in Geosynchronous Earth Orbit (GEO) to serve ten clients with various operational needs (e.g., refueling, relocation), considering both high-thrust and low-thrust propulsion. They solve the combinatorial problem using a genetic algorithm. Similarly, Sarton Du Jonchay et al. [17] expands upon this work by incorporating a detailed case study that accounts for launch costs and the use of multimodal servicers for a GEO satellite servicing mission, solving the combinatorial problem through Mixed-Integer Linear Programming (MILP). However, in these studies, the functional problem considers only phasing maneuvers, and the effect of perturbations is not addressed.

Wijayatunga et al. [11] considers a three-phase-maneuver distance metric including the effects of drag, eclipse power constraints, and fuel mass depletion to obtain the cost and the associated trajectories of a five debris removal mission. Jorgensen and Sharf [12] accurately solve the functional problem by adopting a non-linear programming-based algorithm. The six-element targeting problem is solved for a five debris removal mission. A single-parameter drift orbit is also included to minimize the cost due to RAAN correction. However, in those works the combinatorial problem is not addressed.

Gatto and Casalino [13] solve the optimal sequence problem for a multiple-rendezvous mission involving four asteroids, starting from a dataset of 7075 Near-Earth Asteroids (NEAs). However, the distance metric neglects the fuel mass depletion and can be applied only in the case of small differences in the orbital elements. A similar distance metric is used by Li et al. [14] with the inclusion of the secular J_2 perturbation in the model. The effect of the fuel mass depletion is taken into account by introducing empirical formulas. The optimal tour solution of an active debris removal mission is found. These works neglect both the effect of drag and the propulsion constraint due to eclipse phases.

Narayanaswamy et al. [15] finds the optimal sequence to visit twelve debris by using a simple distance metric that accounts only for inclination and RAAN differences between satellites; then, the optimal-sequence trajectories are obtained by a six-element-targeting feedback controller. Zuiani and Vasile [16] present a solution of an optimal tour problem for an active debris removal mission. The distance metric is derived by assuming averaged dynamics equations and an in-plane control acceleration in order to reduce the number of optimization parameters. However, they do not consider propulsion constraints due to eclipse phases.

Lee and Ahn [18] adopt a two-phase framework to address the optimal multi-target rendezvous problem. Their method combines high-thrust and low-thrust trajectories using an extended Q-law from Varga and Pérez [19]. This framework is applied to an open tour problem involving eight satellites in nearly circular Low Earth Orbit (LEO). The method starts by calculating maneuver costs for the

single-target problem at various departure times. These costs are then used to address the combinatorial problem through Integer Linear Programming (ILP). However, their solution does not account for variations in the servicer's mass during maneuver cost calculations, which can significantly affect the available acceleration, thereby impacting both the total time of flight and fuel consumption. Furthermore, the reliance on ILP introduces limitations, as the method is best suited for scenarios with linear objective functions and constraints.

In previous work, Apa et al. [20] presents a solution to the optimal tour problem, which focuses on visiting forty-one satellites in Medium Earth Orbit (MEO) with a single low-thrust servicing spacecraft. This solution utilizes the Q-law feedback controller proposed by Petropoulos [21] to quantify the cost of five orbital element-targeting maneuvers, while the combinatorial problem is tackled by using MILP. However, the proposed approach does not account for the effects of perturbations.

In this paper, by starting from and expanding upon the approach of Cerf [4], we propose a general approach that can be applied to mission scenarios involving multiple-visitation problems with low-thrust propulsion in the presence of perturbations. In order to solve the functional problem, we adopt a Q-law-based distance metric that incorporates the effects of fuel mass depletion, eclipse caused by Earth's shadow, and secular J_2. Both minimum-time and minimum-fuel problems are considered. All possible visitation costs are computed for a discrete number of servicer masses and departure times. Bilinear interpolation is applied to obtain a quick-to-evaluate continuous approximation of the distance metric. Furthermore, to solve the combinatorial problem, different heuristics are run multiple times to assure the convergence to the global optimal sequence. The performance of a genetic algorithm, simulated annealing, and a particle swarm method are compared with respect to a benchmark problem, where a servicer must visit all clients of a dataset once. A dataset of twenty satellites located between MEO and GEO is considered. The accuracy of the proposed approach is assessed by comparison with respect to a direct optimization method.

The main original contributions of the paper are: 1) A novel method for solving the functional problem is proposed by integrating a distance metric-incorporating eclipse power constraints, fuel mass depletion, secular J_2 effects, and considering both minimum-time and minimum-fuel transfer strategies-with a discretization approach that accounts for variations in the servicer's mass and departure time; and 2) the functional problem is addressed independently and prior to the combinatorial one. This separation allows for flexibility in adapting to various operational constraints-which define different types of multi-client path optimization problems-and supports the use of heuristics for efficiently solving the combinatorial problem, achieving high accuracy in finding the optimal solution while avoiding problem linearization.

The paper is organized as follows. Section 2 reports the problem statement of a generic MTPOP. Section 3 presents the dynamic model. Section 4 introduces the Q-law-based distance metric. In Sect. 5, the time-varying matrix interpolation method is derived. Section 6 examines the combinatorial problem and presents the algorithms for its resolution. In Sect. 7, the proposed approach is applied to a benchmark problem and validated by a direct optimization method. Finally, in Sect. 8, the conclusions are drawn.

2 Moving-Target Path Optimization Problem (MTPOP): Problem Statement

The *"Moving-Target (or time-dependent) Traveling Salesman Problem"* (MTTSP) represents the archetype of multiple-visitation problems where a salesman must visit all cities of a dataset once and only once and the city locations are time-varying. From a mathematical point of view, the MTTSP falls into the class of combinatorial problems, where both integer and continuous variables need to be optimized [22]. The cost of each visitation is quantified by a time-dependent distance metric. MTPOPs represent a more general class of problems where generic constraints and objective function formulation are taken into consideration [4]. The global optimization problem can be mathematically defined by mixing integer variables, real variables, and functions.

Let $\mathcal{K} = \{1, ..., i, ..., N_{sat}\}$ be the set of IDs associated with N_{sat} satellites. A visiting sequence is defined by an ordered set of positive integers $\mathcal{D} = \left\{d_1, ..., d_i, ..., d_{N_d}\right\}, d_i \in \mathcal{K}$ whose components are the IDs of the $N_d \leq N_{sat}$ clients to be visited. Let $\mathbf{ToF} = \left[t_1, ..., t_i, ..., t_{N_d}\right] \in \mathbb{R}^{+N_d}$ be the vector containing the time of each rendezvous between the servicer and the clients. A set of $N_d - 1$ functions $\mathcal{T} = \left\{\mathbf{T}_1(t), ..., \mathbf{T}_i(t), ..., \mathbf{T}_{N_d-1}(t)\right\}$ is used to denote the servicer control law to perform each visitation. Finally, let t_0 be the start time of the mission. In its general form, the MTPOP can be stated as follows

Problem 1 Moving-Target Path Optimization Problem

$$\min_{\mathcal{D},\mathbf{ToF},\mathcal{T}} \sum_{i=1}^{N_d-1} C\left(d_i, d_{i+1}, t_i, t_{i+1}, \mathbf{T}_i(t), \mathbf{p}\right)$$

subject to

$$\begin{aligned}
&\dot{\mathbf{X}}_S(t) = \mathcal{F}\left(\mathbf{X}_S(t), \mathbf{T}_i(t)\right) && \forall t \in [t_0, t_{N_d}], \forall i \in \{1, \dots, N_d - 1\}\\
&\|\mathbf{T}_i(t)\| \leq T_{max} && \forall t \in [t_0, t_{N_d}], \forall i \in \{1, \dots, N_d - 1\}\\
&\dot{\mathbf{X}}_i(t) = \mathcal{G}_i\left(\mathbf{X}_i(t), \mathbf{T}_i^c(t)\right) && \forall t \in [t_0, t_{N_d}], \forall i \in \mathcal{K}\\
&\mathbf{X}_S(t_0) = \mathbf{X}_{S,0}\\
&\mathbf{X}_i(t_0) = \mathbf{X}_{i,0} && \forall i \in \{1, \dots, N_d\}\\
&\mathbf{X}_{S,[1:6]}(t_i) = \mathbf{X}_{d_i,[1:6]}(t_i) && \forall i \in \{1, \dots, N_d\}\\
&d_i \in \mathcal{K} && \forall i \in \{1, \dots, N_d\}\\
&d_i \neq d_j && \forall i, j \in \{1, \dots, N_d\}, i \neq j\\
&t_i \leq t_{i+1} && \forall i \in \{1, \dots, N_d - 1\}\\
&\mathbf{Z}_{eq}\left(\mathcal{D}, \mathbf{ToF}, \mathcal{T}, \mathbf{X}_S, \mathbf{X}_1, \dots, \mathbf{X}_{N_d}\right) = 0\\
&\mathbf{Z}_{ineq}\left(\mathcal{D}, \mathbf{ToF}, \mathcal{T}, \mathbf{X}_S, \mathbf{X}_1, \dots, \mathbf{X}_{N_d}\right) \leq 0
\end{aligned}$$

where T_{max} denotes the maximum available thrust, while C represents the cost associated with transferring from satellite d_i at time t_i to satellite d_{i+1} at time t_{i+1} by the control law $\mathbf{T}_i(t)$. The vector $\mathbf{p}$ encapsulates additional parameters. Furthermore, $\mathbf{X}_S(t)$ denotes the state of the servicer, consisting of the Keplerian elements (semi-major axis, eccentricity, inclination, RAAN, argument of perigee, and true anomaly) and the current mass, $\mathbf{X}_S(t) = [a(t), e(t), i(t), \Omega(t), \omega(t), \theta(t), m(t)]_S^\intercal$; and $\mathbf{X}_i(t)$ represents the state of the i^{th} client. $\mathcal{F}$ and $\mathcal{G}_i$ represent the dynamics of the servicer and the dynamics of the i^{th} client, depending on the control thrusts $\mathbf{T}_i(t)$ and $\mathbf{T}_i^c(t)$, respectively. Initial boundary conditions $\mathbf{X}_{S,0}$ and $\mathbf{X}_{i,0}$ are set, while the rendezvous condition $\mathbf{X}_{S,[1:6]}(t_i) = \mathbf{X}_{d_i,[1:6]}(t_i)$ ensures matching orbital elements at time t_i between the servicer and the client d_i, with the subscript $[1:6]$ indicating equivalence of the first six components. Finally, $\mathbf{Z}_{eq}$ and $\mathbf{Z}_{ineq}$ represent other non-linear equality and inequality constraints involving the sequence, the times of flight, the control laws, and the states of the satellites. The choice of the cost function C (also called distance metric) and the algorithm to find $\mathcal{D}$, **ToF**, and $\mathcal{T}$ will affect both the accuracy of the optimal solution and the computational time.

The problem stated above is intrinsically time-dependent. The satellites are subject to dynamics; if perturbations are included in the propagation model (e.g., J_2, drag, eclipse) the orbits of clients change over time. Furthermore, as the servicer's fuel mass decreases, the available control acceleration varies under the condition of constant thrust. Finally, rendezvous constraints impose that the servicer and each client must have the same orbital elements (or, equivalently, same absolute position and velocity) at time t_i. It is also evident that other time-dependencies can result from equality and inequality constraints.

In the context of low-thrust propulsion, solving the functional problem to derive the optimal-control-theory-based set of functions $\mathcal{T}$ represents the most challenging aspect. The use of optimal computational methodologies, based on Direct Methods (DM) or Indirect Methods (IM) [23] optimization, for the evaluation of the cost associated with the individual leg would be the most natural. These methods succeed in finding the optimal solution but can present some problems such as a restricted convergence domain (especially for IM), the need of an accurate first guess (for DM) [24] and, in general, a relatively high computational cost that makes their application to MTPOPs prohibitive because of the large number of possible sequences to be evaluated.

Another critical aspect involves the combinatorial problem. Sequence optimization algorithms typically fall into two categories: deterministic and heuristic. Deterministic algorithms aim at finding the global optimum and are suitable for small datasets; examples include Exhaustive Search (ES) [25], which evaluates the cost for all possible sequences to determine the global minimum. However, deterministic algorithms incur a significant computational burden that becomes impractical for large datasets. To obtain a feasible solution within reasonable computational time, heuristic algorithms (e.g., greedy algorithm [26], genetic algorithm [27], simulated annealing [28], particle swarm [29]) introduce probability functions to generate sequences for evaluation. Their accuracy depends on user-defined parameters, and global optimality is not assured.

In summary, the problem stated above is difficult to solve, especially when N_{sat} is large. Assumptions are necessary to find computationally viable solutions.

The following assumptions will be adopted from now on:

A.1 **Orbital Transfer**

The phasing cost is neglected, i.e., five orbital-element transfers are considered. Previous studies have demonstrated that the cost difference between a transfer maneuver and a rendezvous maneuver is generally negligible when low-thrust propulsion systems are employed [30]. In particular, the solution of the combinatorial problem is barely affected by the fast variable targeting. This is a usual assumption when dealing with multiple-visitation low-thrust problems [14–16, 31].

A.2 **Distance Metric**

The cost to transfer between a given ordered pair of satellites depends only on their initial states.

This assumption implies that a distance metric form C can be defined a priori for each possible transfer.

The MTPOP is completely defined by the choice of a distance metric and an algorithm to solve the combinatorial path problem. In the following, the dependence of the distance metric on the parameters $\mathbf{p}$ will be assumed and not explicitly underlined.

3 Dynamic Model

Let $\mathbf{T}(t)$ be the control thrust described in the radial, transverse, and out-of-plane (RTN) reference frame. The dynamics of the servicer can be written as

$$\dot{\mathbf{X}}_S(t) = \mathcal{F}(\mathbf{X}_S(t), \mathbf{T}(t)) = \begin{bmatrix} \boldsymbol{A}\frac{w_{ecl}\mathbf{T}}{m} \\ -\frac{\|w_{ecl}\mathbf{T}\|}{g_0 I_{sp}} \end{bmatrix} + \begin{bmatrix} \mathbf{b} \\ 0 \end{bmatrix} + \dot{\mathbf{X}}_{J_2}(t) \tag{1}$$

where $\mathbf{A} \in \mathbb{R}^{6\times3}$ and $\mathbf{b} \in \mathbb{R}^{6\times1}$ represent the contribution of the central body acceleration and $\dot{\mathbf{X}}_{J_2}(t)$ that of the secular J_2 perturbation. Denoting with $p = a(1-e^2)$ the semi-latus rectum, with $h = \sqrt{\mu p}$ the angular momentum, and with r_{SC} the distance of the satellite from the center of the Earth, the following equations hold [32, 33]

$$\mathbf{A} = \begin{bmatrix} \boldsymbol{B} \\ \frac{p\cos(\theta)}{he} & \frac{-(p+r_{SC})\sin(\theta)}{he} & 0 \end{bmatrix} \tag{2}$$

$$\boldsymbol{B} = \begin{bmatrix} \frac{2a^2}{h} e \sin(\theta) & \frac{2a^2}{h} \frac{p}{r_{SC}} & 0 \\ \frac{1}{h} p \sin(\theta) & \frac{1}{h}((p + r_{SC}) \cos(\theta) + r_{SC} e) & 0 \\ 0 & 0 & \frac{r_{SC} \cos(\omega+\theta)}{h} \\ 0 & 0 & \frac{r_{SC} \sin(\omega+\theta)}{h \sin(i)} \\ -\frac{1}{he} p \cos(\theta) & \frac{1}{he}(p + r_{SC}) \sin(\theta) & -\frac{r_{SC} \sin(\omega+\theta)}{h \tan(i)} \end{bmatrix} \tag{3}$$

$$\mathbf{b} = \begin{bmatrix} \mathbf{0}_{5\times1} \\ \frac{h}{r_{SC}^2} \end{bmatrix} \tag{4}$$

$$\dot{\mathbf{X}}_{J_2}(t) = \begin{bmatrix} \mathbf{0}_{3\times1} \\ -\frac{3}{2} J_2 \sqrt{\frac{\mu}{a(t)^3}} \left(\frac{R_e}{p(t)}\right)^2 \cos i(t) \\ \frac{3}{4} J_2 \sqrt{\frac{\mu}{a(t)^3}} \left(\frac{R_e}{p(t)}\right)^2 (5 \cos^2 i(t) - 1) \\ -\frac{3}{4} J_2 \sqrt{\frac{\mu}{a(t)^3}} \left(\frac{R_e}{p(t)}\right)^2 (2 - 3 \sin^2 i(t)) \\ 0 \end{bmatrix} \tag{5}$$

where $g_0 = 9.8066$ m/s^2 is the reference gravitational acceleration, I_{sp} is the specific impulse of the propulsion system, $J_2 = 1.083 \times 10^{-3}$ is the first zonal harmonic coefficient, $\mu = 3.986 \times 10^{14}$ m^3/s^2 is the gravitational constant of the Earth, and $R_e = 6378.137$ km is its mean radius. Equation 3 represents the Gauss Variational Equations (GVEs) for the slow variables. The eclipse effect is represented by the variable $0 \leq w_{ecl} \leq 1$ (its expression can be found in Appendix B).

Equations 1–5 describe the spacecraft dynamics under the assumption that short- and long-period oscillations due to perturbations are neglected. This approximation aligns with the objective of employing a feedback controller (see Sect. 4), as the presence of short-period oscillations would introduce chattering effects that negatively impact the controller's performance. The accuracy of this approximation and its complete derivation can be found in [33].

Considering the eclipse effect is crucial for electric low-thrust propulsion systems, which rely on solar energy to generate thrust. During eclipse phases, energy is stored in the spacecraft's batteries to power critical subsystems, resulting in the deactivation of the thrusters. This aspect has a relevant impact on a transfer maneuver (especially in the time of flight [34]).

Finally, we assume that the satellites to be visited are uncontrolled ($\mathbf{T}_i^c(t) = \mathbf{0}, \forall t$) but subjected to the central body perturbation and secular J_2 perturbation. Their dynamics are governed by the following equation

$$\dot{\mathbf{X}}_i(t) = \mathcal{G}_i(\mathbf{X}_i(t), \mathbf{0}) = \mathcal{F}(\mathbf{X}_i(t), \mathbf{0}) \ \forall i \in \{1, ..., N_{sat}\} \tag{6}$$

If the dynamics $\dot{\mathbf{X}}_i(t)\ \forall t$ and the initial Keplerian elements at the start of the mission t_0 (i.e., $\mathbf{X}_i(t_0)$) are known, the complete state can be obtained at the generic time t as

$$\mathbf{X}_i(t) = \mathbf{X}_i(t_0) + \int_{t_0}^{t} \dot{\mathbf{X}}_i(t)dt \quad \forall i \in \{1, ..., N_{sat}\} \tag{7}$$

4 Distance Metric

In this work, a Q-law-based distance metric is employed to quantify the cost in terms of both fuel and time of flight for a generic transfer maneuver.

4.1 Q-law Overview

Q-law is a closed-loop feedback-driven (CLFD) guidance method, first proposed in [21], based on Lyapunov's second theorem [35]. Let $\overline{\mathbf{X}}(t) = [a(t), e(t), i(t), \Omega(t), \omega(t)]^\intercal$ be the state of the spacecraft represented by the Keplerian elements (neglecting the fast variable θ and the mass m); let $\overline{\mathbf{X}}_T = [a_T, e_T, i_T, \Omega_T, \omega_T]^\intercal$ be a fixed target state; and let $\mathbf{Z} = \overline{\mathbf{X}}(t) - \overline{\mathbf{X}}_T$ be the error state. By using Eqs. 1 and 3, and considering only the central body perturbation, the following equation holds

$$\dot{\mathbf{Z}} = \frac{\partial \mathbf{Z}}{\partial t} = \dot{\overline{\mathbf{X}}}(t) - \dot{\overline{\mathbf{X}}}_T = \dot{\overline{\mathbf{X}}}(t) = \mathbf{B}\mathbf{u}(t) \tag{8}$$

where $\mathbf{u}(t) = \mathbf{T}(t)/m(t)$ is the vector of control acceleration. It is possible to write the time derivative of the general Lyapunov function $Q(\mathbf{Z})$ as

$$\dot{Q}(\mathbf{Z}) = \frac{\partial Q(\mathbf{Z})}{\partial t} = \frac{\partial Q(\mathbf{Z})}{\partial \mathbf{Z}} \frac{\partial \mathbf{Z}}{\partial t} = \frac{\partial Q(\mathbf{Z})}{\partial \mathbf{Z}} \dot{\overline{\mathbf{X}}}(t) = \frac{\partial Q(\mathbf{Z})}{\partial \mathbf{Z}} \mathbf{B}\mathbf{u} \tag{9}$$

For a given Lyapunov function, it is possible to obtain near-optimal minimum-time trajectories by minimizing its time derivative at each instant by choosing

$$\mathbf{u} = -\mathbf{B}^T \frac{\partial Q(\mathbf{Z})}{\partial \mathbf{Z}}^T \tag{10}$$

As proposed in [21], the following Lyapunov function is considered

$$Q(\mathbf{Z}) = \left(1 + W_P P\right) \sum_{i=1}^{5} W_i S_i \left(\frac{\delta Z_i}{\max_\theta(\dot{X}_i)} \right)^2, \quad \boldsymbol{\delta}\mathbf{Z} = \begin{bmatrix} a - a_T \\ e - e_T \\ i - i_T \\ \arccos\left(\cos\left(\Omega - \Omega_T\right)\right) \\ \arccos\left(\cos\left(\omega - \omega_T\right)\right) \end{bmatrix} \tag{11}$$

where $W_P \geq 0, W_i \geq 0$ are user-defined parameters and could be adjusted in order to prioritize the convergence of a particular element, P and S_i are predefined functions, and $\max_\theta(\dot{X}_i)$ is the maximum rate of change of i^{th} orbital element with respect to true anomaly over the current osculating orbit and can be calculated analytically for

all elements except for ω in the case of Keplerian dynamics. The analytical expressions for these terms are provided in Appendix A.

From Eq. 11 it is possible to compute the analytic form of $\partial Q(\mathbf{Z})/\partial \mathbf{Z}$ and from Eq. 10 the control acceleration at each instant by using the osculating orbital elements. It is sufficient to integrate the system starting with initial orbital elements using the control in Eq. 10 in order to drive the satellite to the target; the integration is stopped when $\|\delta Z_i\| \leq \epsilon_i$, $\forall i = \{1, ..., 5\}$ where ϵ_i is the i^{th} orbital element predefined tolerance.

Pontryagin's Principle applied to space trajectories finds that, for Constant Specific Impulse (CSI) propulsion systems, the minimum-time optimal trajectory is composed of maximum-thrust, always-on arcs [36]. It is possible to modify Eq. 10 to consider the maximum available thrust T_{max} as

$$\mathbf{u} = \frac{T_{max}}{m}\left(\frac{-\mathbf{B}^T \frac{\partial Q(\mathbf{Z})}{\partial \mathbf{Z}}^T}{\|\mathbf{B}^T \frac{\partial Q(\mathbf{Z})}{\partial \mathbf{Z}}^T\|}\right) = \frac{T_{max}}{m}\begin{bmatrix}\sin(\alpha)\cos(\beta)\\ \cos(\alpha)\cos(\beta)\\ \sin(\beta)\end{bmatrix} = \frac{T_{max}}{m}\hat{\mathbf{u}} \tag{12}$$

Here, α and β denote the in-plane and out-of-plane angles of the thrust, respectively. These angles are illustrated in Fig. 1 in the RTN reference frame, represented by the unit vectors $\hat{e}_R$, $\hat{e}_T$, and $\hat{e}_N$.

For minimum-fuel optimal trajectories, Pontryagin's Principle finds that the solution is composed of maximum-thrust arcs and thrust-off arcs (coast arcs) [37]. This aspect is taken into account by the introduction of two additional parameters, the so-called relative and absolute effectivities (η_r and η_a). These parameters introduce coast arcs at points along the orbit where the engine thrust is less efficient; they are defined as [38]

$$\eta_a = \frac{\min_{\alpha,\beta}(\dot{Q})}{\min_\theta\left(\min_{\alpha,\beta}(\dot{Q})\right)},\ \eta_r = \frac{\min_{\alpha,\beta}(\dot{Q}) - \max_\theta\left(\min_{\alpha,\beta}(\dot{Q})\right)}{\min_\theta\left(\min_{\alpha,\beta}(\dot{Q})\right) - \max_\theta\left(\min_{\alpha,\beta}(\dot{Q})\right)} \tag{13}$$

where $\min_{\alpha,\beta}(\dot{Q})$ is the minimum of the Lyapunov function with respect to α and β evaluated at the osculating orbital elements and can be computed as

$$\min_{\alpha,\beta}(\dot{Q}) = \min_{\alpha,\beta}\left(\left(\frac{\partial Q}{\partial \boldsymbol{Z}}\right)\boldsymbol{B}\boldsymbol{u}\right) = -\left\|\boldsymbol{B}^T\left(\frac{\partial Q}{\partial \boldsymbol{Z}}\right)^T\right\|$$

while $\min_\theta\left(\min_{\alpha,\beta}(\dot{Q})\right)$ and $\max_\theta\left(\min_{\alpha,\beta}(\dot{Q})\right)$ are respectively the minimum and the maximum of the time derivative of the Lyapunov function with respect to α, β and θ over an entire orbit ($\theta \in [0, 2\pi]$); these quantities can not be expressed in closed form and they have to be obtained numerically (for example through a grid search algorithm). η_r and η_a attempt to quantify the effectiveness of changing the orbital parameters at a given osculating point compared to the optimum point for changing the orbital parameters over a complete orbit. When some thresholds are set ($\overline{\eta}_r$, $\overline{\eta}_a$), the control law follows

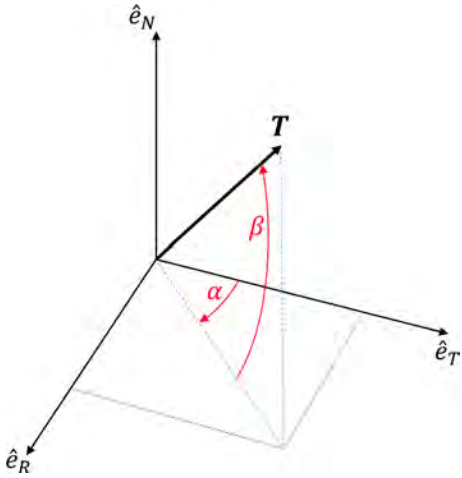

Fig. 1 Illustration of the in-plane angle α and out-of-plane angle β of the thrust

$$\mathbf{u} = \begin{cases} \mathbf{0} & if \quad \eta_r \leq \overline{\eta}_r \quad or \quad \eta_a \leq \overline{\eta}_a \\ \frac{T_{max}}{m} \begin{bmatrix} \sin(\alpha)\cos(\beta) \\ \cos(\alpha)\cos(\beta) \\ \sin(\beta) \end{bmatrix} & otherwise \end{cases} \tag{14}$$

The control thrust can be computed from Eqs. 12 and 14 for minimum-time and minimum-fuel scenarios, respectively, as

$$\mathbf{T}(t) = m(t)\mathbf{u}(t) \tag{15}$$

Equations 12 and 14 represent a near-optimal solution of the functional problem respectively in minimum-time and minimum-fuel scenarios.

Q-law cannot be used in any of its forms where the time of flight is prescribed. The time of flight and the fuel depletion are a direct consequence of the weights, the stopping criteria, and the effectivity thresholds.

Q-law does not account for perturbations (i.e., $\mathbf{B}(t)$ represents the dynamics equation for Keplerian motion). However, its closed-loop feedback nature allows the use of osculating orbital elements coming from the propagation of the perturbed dynamics [39]. In particular, the same form of Eqs. 10 and 11 is maintained and evaluated at the servicer and target perturbed states $\mathbf{X}(t)$ and $\mathbf{X}_T(t)$ computed by Eqs. 1 and 6.

4.2 Q-law-Based Distance Metric

For a given propulsion system, characterized by T_{max} and I_{sp}, and a specified mission start time t_0, the Q-law allows the computation of the velocity increment (ΔV) and the time of flight (ToF) for each possible transfer. This calculation requires the selection of user-defined Q-law parameters (i.e., weights W_P and W_i, stopping criteria ϵ_i, effectivities thresholds $\overline{\eta}_r, \overline{\eta}_a$) and the transfer type

(minimum-time or minimum-fuel). Specifically, the values of ΔV and ToF are obtained as follows

$$\Delta V(t_i, m_i, d_j, d_k) = \int_{t_i}^{t_f(t_i,m_i,d_j,d_k)} \mathbf{u}(t)dt \tag{16}$$

$$ToF(t_i, m_i, d_j, d_k) = t_f(t_i, m_i, d_j, d_k) - t_i \tag{17}$$

where t_i is the departure time computed from t_0, m_i is the initial mass of the servicer, d_j and d_k are the indexes referring respectively to the initial and target orbit, and $\mathbf{u}(t)$ is computed by Eq. 12 or Eq. 14. The initial state of the servicer for integration within the Q-law algorithm is derived by propagating the Keplerian elements associated with index d_j through Eqs. 6 and 7, evaluated at time t_i. The integration terminates at time t_f (corresponding to the arrival time at the target orbit d_k) once the stopping criteria ϵ_i are satisfied.

From Eqs. 16 and 17, a distance metric in the form reported in Sect. 2 (i.e., $C\big(d_i, d_j, t_i, t_j, \mathbf{T}(t)\big)$) can be constructed.

5 General Approach: Time-Varying Matrix Interpolation

The *Time-Varying Matrix Interpolation* (TVMI) method is here proposed to find a solution to general optimal path problems within reasonable computational times. The approach is composed of two steps:

1. Cost-Array Computation
2. Bilinear Interpolation

The output of the procedure is an approximate, yet quick-to-evaluate, distance metric that accounts for time dependencies. As a result, the MTPOP reduces to a combinatorial problem (Sect. 6).

5.1 Cost-Array Computation

In previous sections, two four-variable functions were derived (Eqs. 16 and 17). In a real mission scenario, the servicer total mass m_0, the dry mass of the servicer m_{dry}, the start time t_0 and the maximum total mission duration Δt_M are either known or design quantities. By defining the continuous closed intervals $M_C = [m_{dry}, m_0]$ and $T_C = [t_0, t_0 + \Delta t_M]$, the number of mass points N_M and the number of time points N_T, M_C and T_C can be discretized as follows

$$\begin{aligned} M_D &= \{M_1, ..., M_{N_M+1}\}, & M_i &= m_{dry} + (i-1)\tfrac{m_0 - m_{dry}}{N_M} & \forall i \in \{1, ..., N_M + 1\} \\ T_D &= \{T_1, ..., T_{N_T+1}\}, & T_l &= t_0 + (l-1)\tfrac{\Delta t_M}{N_T} & \forall l \in \{1, ..., N_T + 1\} \end{aligned} \tag{18}$$

Eq. 18 represents a discretization of the intervals M_C and T_C in $N_M + 1$ and $N_T + 1$ points, respectively. Starting from Eqs. 16, 17, and 18 two four-dimensional arrays ($\Delta V_{D,iljk}$ and $ToF_{D,iljk}$) can be computed as follows

$$\Delta V_{D,iljk} = \Delta V(M_i, T_l, d_j, d_k) \qquad \begin{aligned} &\forall i \in \{1, ..., N_M + 1\} \\ &\forall l \in \{1, ..., N_T + 1\} \\ &\forall j, k \in \{1, ..., N_{sat}\} \end{aligned} \tag{19}$$

$$ToF_{D,iljk} = ToF(M_i, T_l, d_j, d_k) \qquad \begin{aligned} &\forall i \in \{1, ..., N_M + 1\} \\ &\forall l \in \{1, ..., N_T + 1\} \\ &\forall j, k \in \{1, ..., N_{sat}\} \end{aligned} \tag{20}$$

Due to the time-dependency, a permutation of d_j and d_k in Eqs. 16 and 17 does not yield the same results (i.e., $\Delta V(t_i, m_i, d_j, d_k) \neq \Delta V(t_i, m_i, d_k, d_j)$ and $ToF(t_i, m_i, d_j, d_k) \neq ToF(t_i, m_i, d_k, d_j)$). Considering that in case $j = k$, the initial orbit coincides with the final orbit (i.e., $\Delta V = ToF = 0$), computing Eqs. 19 and 20 requires a number of Q-law evaluations, which is given by Eq. 21.

$$z = \left(N_M + 1\right)\left(N_T + 1\right)\left(N_{sat} - 1\right)N_{sat} \tag{21}$$

The arrays $\Delta V_{D,iljk}$ and $ToF_{D,iljk}$ contain the costs, respectively, in terms of fuel and time of flight, obtained by solving the functional problem for all possible transfers between the satellites in a given dataset, considering a finite number of servicer initial masses and departure times.

Figure 2 shows a conceptual visualization of the $\Delta V_{D,iljk}$ array in the case of $N_{sat} = 3$, $N_M = 3$, and a generic N_T. Each element of the array is obtained by solving the functional problem. Colors represent different values of ΔV. The same schematic decomposition can be applied to $ToF_{D,iljk}$.

5.2 Bilinear Interpolation

In real applications, both the initial mass of the servicer and departure time can assume any values within specified continuous intervals. Starting from the pre-computed arrays (Eqs. 19 and 20), two mapping functions $f_{\Delta V,jk} : \mathbb{R}^2 \to \mathbb{R}$ and $f_{ToF,jk} : \mathbb{R}^2 \to \mathbb{R}$, operating on the sub-matrices $\Delta V_{D,jk} := \Delta V_{D,iljk}, \forall i, l$ and $ToF_{D,jk} := ToF_{D,iljk}, \forall i, l$, can be defined to obtain an approximation of the costs on the continuous closed intervals M_C and T_C previously introduced. The following equations hold

$$\Delta V_{C,jk} = \Delta V_{C,jk}\left(t_i, m_i, d_j, d_k\right) = f_{\Delta V,jk}\left(t_i, m_i\right) \quad \forall t_i \in T_C, \forall m_i \in M_C \tag{22}$$

$$ToF_{C,jk} = ToF_{C,jk}\left(t_i, m_i, d_j, d_k\right) = f_{ToF,jk}\left(t_i, m_i\right) \quad \forall t_i \in T_C, \forall m_i \in M_C \tag{23}$$

Equations 22 and 23 refer to the costs associated with the transfer between the d_j and d_k satellites of the dataset. The complete set of mapping functions is defined for

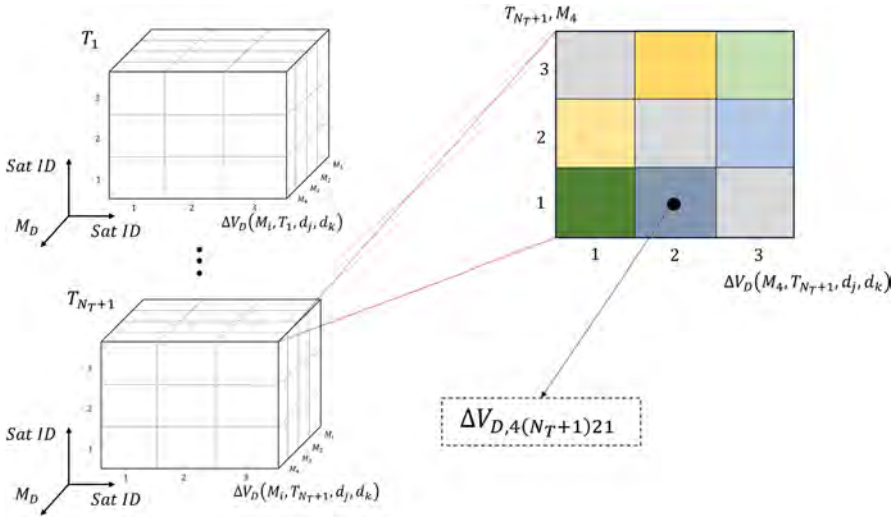

Fig. 2 $\Delta V_{D,iljk}$ array decomposition

all possible transfers as $f_{\Delta V,jk}, \forall j,k \in \{1,...,N_{sat}\}$ and $f_{ToF,jk}, \forall j,k \in \{1,...,N_{sat}\}$. In this work, $f_{\Delta V,jk}$ and $f_{ToF,jk}$ are chosen as bilinear interpolating functions, as follows [40]

$$f_{\Delta V,jk}(t_i, m_i) = \frac{1}{(T_{l+1} - T_l)(M_{i+1} - M_i)} \begin{bmatrix} T_{l+1} - t_i \\ t_i - T_l \end{bmatrix}^{\mathsf{T}} \times \begin{bmatrix} \Delta V_{D,iljk} & \Delta V_{D,i(l+1)jk} \\ \Delta V_{D,(i+1)ljk} & \Delta V_{D,(i+1)(l+1)jk} \end{bmatrix} \begin{bmatrix} M_{i+1} - m_i \\ m_i - M_i \end{bmatrix} \tag{24}$$

$$f_{ToF,jk}(t_i, m_i) = \frac{1}{(T_{l+1} - T_l)(M_{i+1} - M_i)} \begin{bmatrix} T_{l+1} - t_i \\ t_i - T_l \end{bmatrix}^{\mathsf{T}} \times \begin{bmatrix} ToF_{D,iljk} & ToF_{D,i(l+1)jk} \\ ToF_{D,(i+1)ljk} & ToF_{D,(i+1)(l+1)jk} \end{bmatrix} \begin{bmatrix} M_{i+1} - m_i \\ m_i - M_i \end{bmatrix} \tag{25}$$

Equations 24 and 25 are presented for the case where t_i and m_i belong to the intervals $T_l \le t_i \le T_{l+1}$ and $M_i \le m_i \le M_{i+1}$, respectively. The same applies to all contiguous subintervals in the discrete sets T_D and M_D.

6 Combinatorial Problem

The TVMI method provides two models, $\Delta V_{C,jk}$ and $ToF_{C,jk}$, representing an approximate solution of the functional problem. The dynamics and the optimization variables $\mathcal{T}$ are included in the models thus reducing the MTPOP to a combinatorial problem, which can be stated as follows

Problem 2 Combinatorial MTPOP

$$\min_{\mathcal{D}} \sum_{j=1}^{N_d-1} D\left(\Delta V_{C,j(j+1)}\left(t_{i,j}, m_{i,j}, d_j, d_{j+1}\right), ToF_{C,j(j+1)}\left(t_{i,j}, m_{i,j}, d_j, d_{j+1}\right)\right)$$

subject to

$$\begin{aligned}\mathbf{Z}_{eq}\left(\mathcal{D}, t_{i,1}, \ldots, t_{i,N_d}, m_{i,1}, \ldots, m_{i,N_d}\right) &= 0\\ \mathbf{Z}_{ineq}\left(\mathcal{D}, t_{i,1}, \ldots, t_{i,N_d}, m_{i,1}, \ldots, m_{i,N_d}\right) &\leq 0\end{aligned}$$

where $\mathcal{D}$ has the same meaning as in Problem 1. D indicates a generic function describing the cost to transfer from d_j to d_{j+1}, while $\mathbf{Z}_{eq}$ and $\mathbf{Z}_{ineq}$ represent generic equality and inequality constraints.

The combinatorial MTPOP stated above can describe a great variety of real mission scenarios. Its domain of validity is only constrained by the assumptions made to derive the two models $\Delta V_{C,jk}$ and $ToF_{C,jk}$.

In this paper, we adapt the general MTPOP framework to focus on a specific case: the optimal open tour problem. In this scenario, the servicer, initially positioned on a given orbit $\overline{d} \in \{1, \ldots, N_{sat}\}$, must visit each satellite exactly once while minimizing the total fuel consumption. This specific adaptation is detailed in the problem statement below.

Problem 3 Open Tour Problem

$$\min_{\mathcal{D}} \sum_{j=1}^{N_{sat}-1} m_{i,j}\left(1 - e^{-\frac{\Delta V_{C,j(j+1)}\left(t_{i,j}, m_{i,j}, d_j, d_{j+1}\right)}{I_{sp} g_0}}\right)$$

subject to

$$
\begin{aligned}
& t_{i,1} = t_0 \\
& m_{i,1} = m_0 \\
& t_{i,j+1} = t_{i,j} + ToF_{C,j(j+1)}\left(t_{i,j}, m_{i,j}, d_j, d_{j+1}\right) && \forall j \in \{1, \ldots, N_{sat} - 1\} \\
& m_{i,j+1} = m_{i,j} \cdot e^{-\frac{\Delta V_{C,j(j+1)}\left(t_{i,j}, m_{i,j}, d_j, d_{j+1}\right)}{I_{sp} g_0}} && \forall j \in \{1, \ldots, N_{sat} - 1\} \\
& m_{i,j} \geq m_{dry} && \forall j \in \{1, \ldots, N_{sat}\} \\
& \mathcal{D} = \{d_1, \ldots, d_{N_{sat}}\} \\
& d_j \in \{1, \ldots, N_{sat}\} && \forall j \in \{1, \ldots, N_{sat}\} \\
& d_1 = \overline{d} \\
& d_j \neq d_k && \forall j, k \in \{1, \ldots, N_{sat}\}, j \neq k
\end{aligned}
$$

As discussed in Sect. 2, both deterministic and heuristic algorithms can be applied to solve Problem 3. For small datasets, ES is effective for identifying the globally optimal sequence. For larger instances with more satellites, heuristic methods are advantageous as they provide solutions within a reasonable time frame.

In this work, three heuristic methods-namely, genetic algorithm, simulated annealing, and particle swarm-are used and compared. The computational efficiency in evaluating the models $\Delta V_{C,jk}$ and $ToF_{C,jk}$ makes it possible to run the algorithms multiple times to verify convergence to the global optimum. A brief overview of these methods is given below.

(a) **Genetic Algorithm**

In this work, a genetic algorithm with mutation is used [27]. The number of members of a population N_{pop}, the maximum number of generations N_{gen}, and maximum number of stall generations N_{stall} are the user-defined parameters. After each generation, the sequence associated with the minimum cost is selected and saved in case of an improvement in the objective function.

(b) **Simulated Annealing**

Simulated annealing is an iterative algorithm to perform global optimization [28]. The initial temperature T_{K0}, the cooling rate R_c, the number of iterations N_{it}, and the number of elements to swap at each iteration N_{swap} are the user-defined parameters.

(c) **Particle Swarm**

Particle swarm is a bio-inspired ensemble learning algorithm to perform global optimization [29]. Similar to the genetic algorithm N_{pop}, N_{gen}, and N_{stall} are the number of members of a population, the maximum number of generations, and the maximum number of stall generations, respectively. The hyperparameters are indicated using b_{1N}, c_1, and c_2, where b_{IN} denotes the inertia weight and the parameters related to cognition and social influence are respectively c_1 and c_2.

Table 1 Satellites' initial Keplerian elements

ID	a[km]	e	i[deg]	Ω[deg]	ω[deg]	θ[deg]
Satellite - 1	22164.8	0.050	3.250	291.6	10.00	30.17
Satellite - 2	23166.7	0.070	5.950	298.2	10.00	100.8
Satellite - 3	25164.8	0.050	7.510	298.0	50.00	78.52
Satellite - 4	26158.9	0.080	9.130	303.4	20.00	240.3
Satellite - 5	28166.7	0.100	2.180	67.46	10.00	330.5
Satellite - 6	29180.4	0.060	10.84	310.1	20.00	200.2
Satellite - 7	30158.9	0.090	9.850	305.6	0.002	150.2
Satellite - 8	31162.8	0.080	11.67	315.2	37.00	300.6
Satellite - 9	32158.9	0.110	13.63	324.4	180.0	175.9
Satellite - 10	33166.7	0.120	13.36	335.4	20.00	286.2
Satellite - 11	34164.8	0.090	15.01	10.09	280.0	45.23
Satellite - 12	35162.8	0.070	13.96	342.3	240.0	123.5
Satellite - 13	36158.9	0.120	13.73	340.1	210.0	91.22
Satellite - 14	37164.7	0.150	14.00	343.8	36.50	210.4
Satellite - 15	38162.8	0.050	9.740	305.5	8.020	350.1
Satellite - 16	39158.9	0.050	14.47	348.9	22.00	250.1
Satellite - 17	40162.8	0.090	14.66	15.07	8.800	35.11
Satellite - 18	41166.7	0.120	14.91	357.2	72.50	60.11
Satellite - 19	42164.8	0.100	14.89	358.9	35.00	70.11
Satellite - 20	43166.7	0.060	14.92	9.420	85.00	10.11

Table 2 Inertial and low-thrust propulsion servicer properties

I_{sp} [s]	T_{max} [N]	m_0 [kg]
2000	2	2000

7 Simulation Results

The proposed methodology was applied to a multiple-visitation application case on a set of $N_{sat} = 20$ MEO/GEO satellites. Their orbital elements at the mission start time are reported in Table 1 while the initial mass and low-thrust propulsion system properties of the servicer [38] are reported in Table 2.

7.1 Solution of the Functional Problem

The dynamics model presented in Sect. 3 was integrated using the control accelerations computed by the Q-law, both in the minimum-time and minimum-fuel scenarios, to compute the arrays (Eqs. 19 and 20) by means of Eqs. 16 and 17. Tables 3 and 4 report respectively the Q-law user-defined parameters and the data used in the array computation. These parameters were selected by a trial-and-error procedure on a sample transfer maneuver. They proved to be a good choice in terms of Q-law

Table 3 Q-law weights, stopping criteria tolerances and effectivities thresholds

W_P	W_i	ϵ_1 [km]	ϵ_2	ϵ_3 [deg]	ϵ_4 [deg]	ϵ_5 [deg]	$\overline{\eta}_r$	$\overline{\eta}_a$
1	[1, 1, 1, 1, 1]	$0.001a_f$	$0.1e_f$	0.1	0.1	0.1	0.25	0.25

Table 4 Array computation data

Mission start date	m_{dry} [kg]	t_0 [days]	Δt_m [days]	N_M	N_T
$01-Jan-2023\,06:00:00$	1000	0	950	19	38

convergence computational time. In principle, they can be optimized for each possible transfer at the expense of increased computational burden. In Table 3, a_f and e_f indicate the stopping criteria tolerances on semi-major axis and eccentricity, set as a fraction of the targeted values.

The computation involved 296, 400 system integrations per case (see Eq. 21), either minimum-time or minimum-fuel. All the computations were conducted in MATLAB [41]. The built-in function *ode113* with a relative tolerance of 1×10^{-7} was used requiring 2.62 h and 4.85 h for the minimum-time and minimum-fuel cases, respectively. All numerical simulations were conducted using parallel computing, implemented through the MATLAB *parfor* keyword to specify parallel for-loops. The computations were performed on a laptop equipped with an 11th Gen Intel(R) Core(TM) i7 processor (2.3 GHz) with 8 physical cores, running a 64-bit Windows operating system and 32 GB of RAM.

7.1.1 Example of Bilinear Interpolation

Figures 3 and 4 show an example of bilinear interpolation for the transfer between satellites 15 and 1. The initial Keplerian elements of these satellites are provided in Table 1. The mapping functions $f_{\Delta V,jk}$ and $f_{ToF,jk}$ were applied to pre-computed arrays, which were derived from the data outlined in Table 4. The servicer propulsion system's maximum thrust and specific impulse match those reported in Table 2. Each element of the arrays was computed by executing the Q-law within the minimum-time framework, using the parameters defined in Table 3. In this example, the computation required approximately 30 seconds.

From Fig. 3 two main findings can be obtained. First, the ΔV needed is slightly dependent on initial mass. Second, the ΔV needed initially increases for increasing values of the departure time, reaching a plateau for values between 600 days and 950 days, indicating that the satellites are drifting apart because of the differential nodal precession; it becomes more efficient to visit the satellite at the beginning of the mission where the $\Delta\Omega$ is lower. Figure 4 shows that a lower initial mass (i.e., greater available acceleration) generally results in shorter times of flight. By accounting for transfer cost variations with mass, the proposed method effectively addresses time-of-flight fluctuations. These

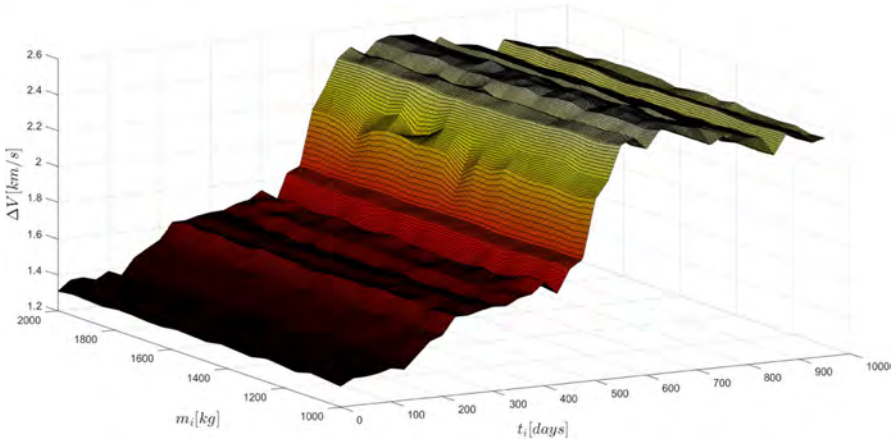

Fig. 3 $\Delta V_{C,jk}$ bilinear interpolation example, $j = 15$ and $k = 1$

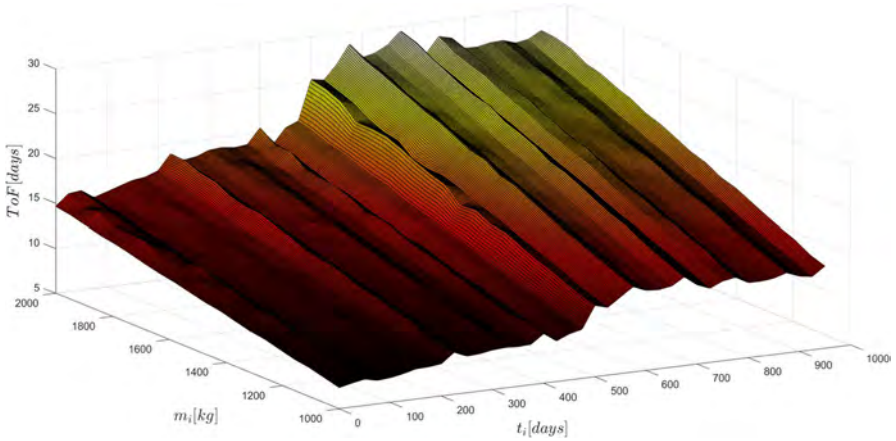

Fig. 4 $ToF_{C,jk}$ bilinear interpolation example, $j = 15$ and $k = 1$

fluctuations significantly impact mission duration, especially as the number of satellites increases and servicer mass variation becomes substantial.

It is clear that a finer discretization would increase both the accuracy of the bilinear interpolation and the computational time required to create $\Delta V_{D,iljk}$ and $ToF_{D,iljk}$, making the choice of N_M and N_T mainly dictated by a trade-off between these two quantities. The main advantage of this approach lies in the possibility of quickly evaluating the $\Delta V_{C,jk}$ and $ToF_{C,jk}$ functions, making the combinatorial path problem easily solvable.

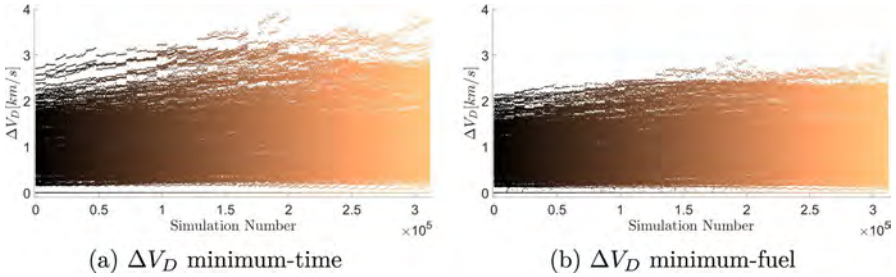

Fig. 5 ΔV_D array inspection

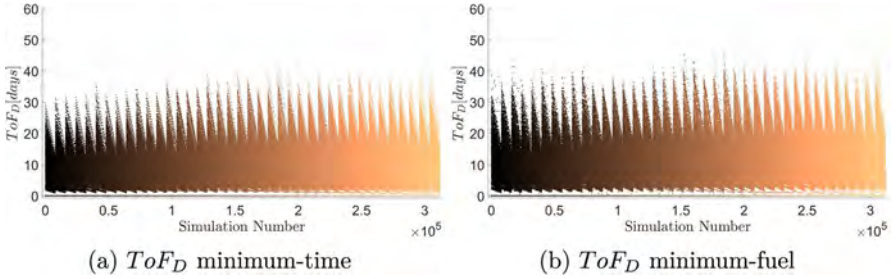

Fig. 6 ToF_D array inspection

7.1.2 Cost-Array Inspection

Figures 5 and 6 show the elements of $\Delta V_{D,jk}$ and $ToF_{D,jk}$ matrices $\forall j,k \in \{1,...,N_{sat}\}$, covering both the minimum-time and minimum-fuel scenarios. In these figures, the same color is assigned to the simulations with the same initial mass and departure time, across all possible combinations of j and k. This color consistency creates vertical bands, where differences in cost due to varying j and k (i.e., different initial and target orbits) are visible along the vertical axis; zero values associated with $j = k$ cases are also plotted. Figure 5 shows that most transfers have costs between 0.1 and 2.5 km/s, with the highest costs reaching approximately 4.0 km/s. Variation in the ΔV range along the x-axis provides insights into how the dispersion of Keplerian elements of satellites changes with variations in the servicer's initial mass and departure time. Comparison of ΔV and time of flight across minimum-time and minimum-fuel scenarios shows that coasting, while reducing fuel consumption, leads to longer flight durations. Specifically, in the minimum-time scenario (Fig. 5a), the ΔV range is broader compared to the minimum-fuel scenario (Fig. 5b), where ΔV values exhibit a narrower range along the vertical axis. Conversely, the time-of-flight range is wider in the minimum-fuel scenario (Fig. 6b), reflecting the additional time required due to periods of thruster inactivity during the transfer.

7.1.3 Bilinear Interpolation Accuracy Analysis

The accuracy of the bilinear interpolation was evaluated using a different discretization of the intervals M_C and T_C. To assess the potential errors between the interpolated values and those obtained through a direct application of the Q-law, two validation matrices ($\Delta V_{val,jk}$ and $ToF_{val,jk}$) were computed for all possible transfers, employing the same parameters as in Tables 2, 3, and 4, with the exception of N_M and N_T (where $N_M = N_T = 4$). The validation sets, denoted by $M_{D,val}$ and $T_{D,val}$, were then used to calculate the percentage error for each sample using the following equations

$$\Delta V_{err} = \frac{|\Delta V_{C,jk}(t_i, m_i, d_j, d_k) - \Delta V_{val,jk}(t_i, m_i, d_j, d_k)|}{\Delta V_{val,jk}(t_i, m_i, d_j, d_k)} \cdot 100 \quad \forall t_i \in T_{D,val} \; \forall m_i \in M_{D,val} \; \forall j,k \in \{1, ..., N_{sat}\}$$

$$ToF_{err} = \frac{|ToF_{C,jk}(t_i, m_i, d_j, d_k) - ToF_{val,jk}(t_i, m_i, d_j, d_k)|}{ToF_{val,jk}(t_i, m_i, d_j, d_k)} \cdot 100 \quad \forall t_i \in T_{D,val} \; \forall m_i \in M_{D,val} \; \forall j,k \in \{1, ..., N_{sat}\}$$

Figure 7 shows the results for all samples in the minimum-time case. In particular, the top and bottom left plots report the percentage errors while the absolute ΔV and ToF values are reported in the top and bottom right plots. The absolute ΔV and ToF are denoted as *Interpolated* for the values obtained by interpolating and

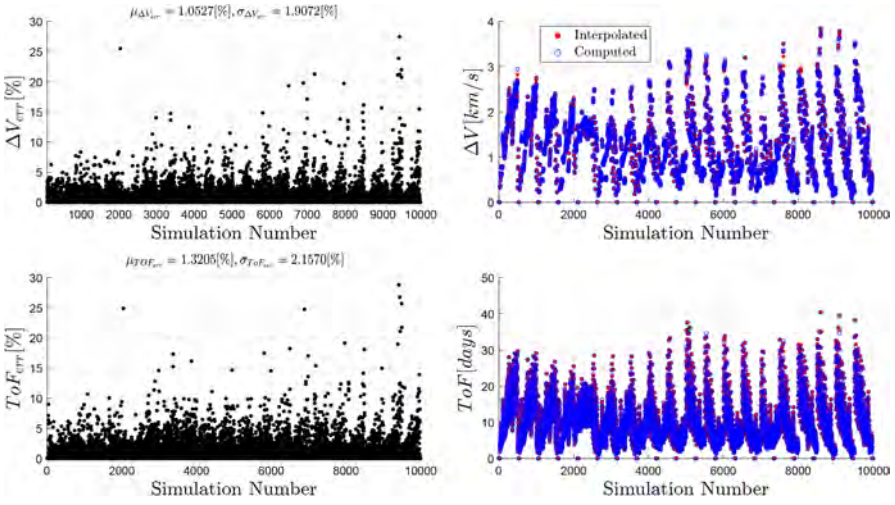

Fig. 7 Validation set results

evaluating the elements of the arrays described in Sect. 7.1.2 at the validation sets $T_{D,val}$ and $M_{D,val}$, while they are referred as *Computed* to denote the values obtained by direct evaluation of the Q-law.

Very few cases are associated with a large percentage error, and the estimations are accurate as demonstrated by the distribution mean and standard deviation values ($\mu_{\Delta V_{err}} = 1.0527$ %, $\sigma_{\Delta V_{err}} = 1.9072$ % and $\mu_{ToF_{err}} = 1.3205$ %, $\sigma_{ToF_{err}} = 2.1570$ %). The accuracy noted in the minimum-time case is also similar in the minimum-fuel scenario, further emphasizing the robustness of the method.

7.2 Solution of the Combinatorial Problem

The open tour problem (Problem 3) was solved using the genetic algorithm, simulated annealing, and particle swarm optimization. The user-defined parameters for these algorithms are detailed in Table 5. Additionally, the servicer was considered to depart from the orbit of satellite 1 (i.e., $\overline{d} = 1$, see Table 1), with a total mass m_0 at start time t_0 as specified in Table 2 and Table 4, respectively.

Each algorithm was executed $N_{run} = 100$ times in parallel for both the minimum-time and minimum-fuel cases. This choice of N_{run} balances the computational expense with the need to mitigate the stochastic nature of the algorithms. The best sequence across all 100 runs was selected, thereby ensuring the accuracy of the results while keeping the computational effort manageable.

Table 6 reports the CPU time, the optimal sequence, the costs associated with the optimal tour in terms of both total fuel consumption and total time of flight, and their absolute percentage errors with respect to the non-interpolated function (i.e., the results of the Q-law computed for the optimal sequence) obtained by the heuristics. Notably, the CPU time is lower than 5 min for all simulations. The genetic algorithm found the sequences associated with the minimum objective function in spite of a greater computational time. The absolute percentage errors remain coherent with the values of mean and standard deviations reported for the validation set (Sect. 7.1.3). The optimal sequence is the same for the two cases, meaning that longer times of flight (due to coast arcs for the minimum-fuel case) are not sufficient to let the perturbations modify the orbital elements significantly.

Figures 8 and 9 show the Keplerian elements history of both minimum-time and minimum-fuel optimal sequences found by the genetic algorithm. It is evident that the sequence of visited clients is characterized by an almost monotonically increasing RAAN relative to the initial location of the servicer. This behavior, referred to as *RAAN walk* [42], is consistent with the fact that RAAN correction requires a large amount of fuel. In Fig. 10, the mass depletion comparison between the two cases

Table 5 Heuristics simulation parameters

Genetic Algorithm			Simulated Annealing				Particle Swarm			
N_{pop}	N_{gen}	N_{stall}	T_{K0}	R_C	N_{it}	N_{swap}	N_{pop}	N_{gen}	N_{stall}	$[b_{IN}, c_1, c_2]$
25	500	50	3000	0.5	5000	5	25	500	50	[0.9, 1, 1]

Table 6 Optimal sequence results and validation

Genetic Algorithm						
Simulation	CPU time [s]	Optimal sequence	ΔM_{tot} [kg]	ToF_{tot} [days]	$\Delta M_{tot,err}$ [%]	$ToF_{tot,err}$ [%]
Minimum time	241.6	{1, 2, 3, 4, 7, 6, 8, 15, 9, 13, 12, 10, 14, 16, 19, 18, 20, 17, 11, 5}	628.0	72.41	1.32	1.56
Minimum fuel	235.1	{1, 2, 3, 4, 7, 6, 8, 15, 9, 13, 12, 10, 14, 16, 19, 18, 20, 17, 11, 5}	560.0	91.67	0.38	2.19
Simulated Annealing						
Simulation	CPU time [s]	Optimal sequence	ΔM_{tot} [kg]	ToF_{tot} [days]	$\Delta M_{tot,err}$ [%]	$ToF_{tot,err}$ [%]
Minimum time	200.1	{1, 2, 4, 3, 15, 7, 6, 8, 9, 10, 12, 13, 14, 16, 11, 18, 19, 17, 20, 5}	725.7	83.75	0.46	0.87
Minimum fuel	229.4	{1, 2, 3, 4, 7, 6, 8, 9, 15, 10, 14, 16, 18, 19, 17, 20, 11, 12, 13, 5}	593.1	95.88	1.93	2.62
Particle Swarm						
Simulation	CPU time [s]	Optimal sequence	ΔM_{tot} [kg]	ToF_{tot} [days]	$\Delta M_{tot,err}$ [%]	$ToF_{tot,err}$ [%]
Minimum time	177.3	{1, 2, 6, 8, 10, 14, 16, 18, 19, 17, 20, 11, 12, 13, 9, 15, 7, 4, 3, 5}	692.5	80.71	0.03	0.61
Minimum fuel	166.3	{1, 2, 3, 4, 7, 6, 8, 15, 9, 13, 12, 11, 17, 20, 19, 18, 16, 14, 10, 5}	562.9	93.97	1.18	2.64

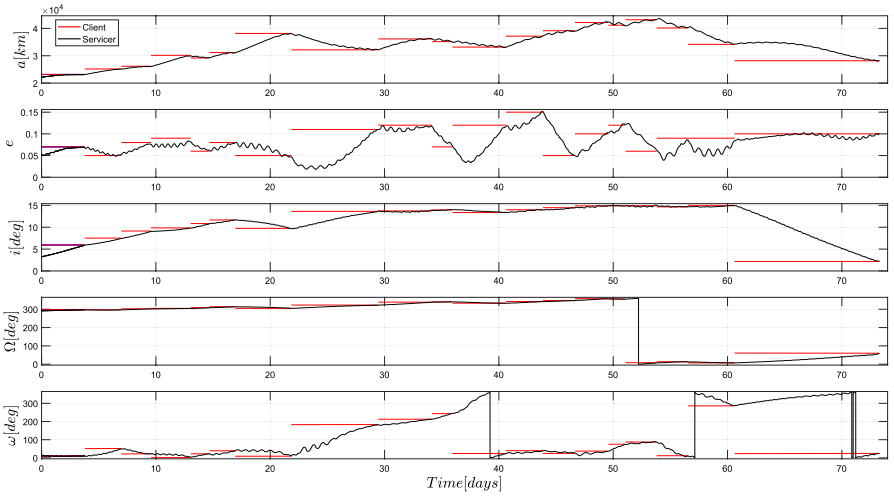

Fig. 8 Optimal sequence Keplerian elements history (minimum-time)

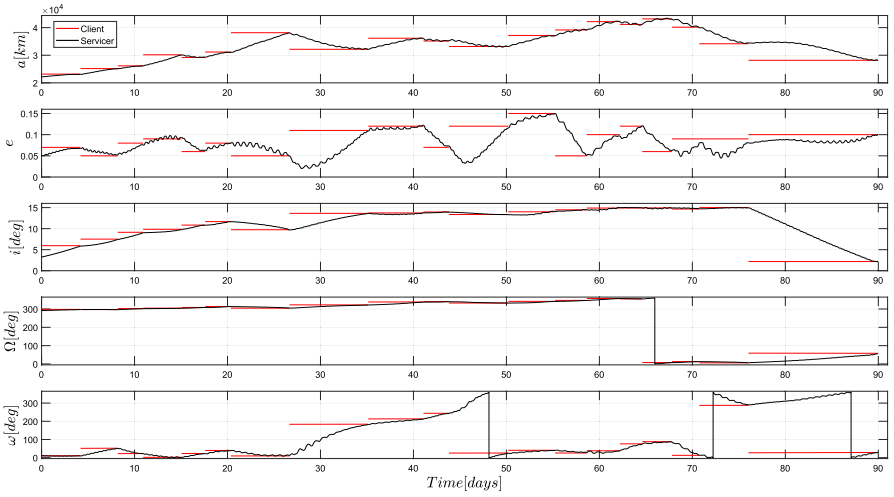

Fig. 9 Optimal sequence Keplerian elements history (minimum-fuel)

is shown (visitation instants are indicated by red dots). In the minimum-time case, fuel decreases almost linearly because the thrust is always on and constant (except when in eclipse). Conversely, in the minimum-fuel case, the coast arc mechanism reduces fuel consumption, though this results in a longer mission duration compared

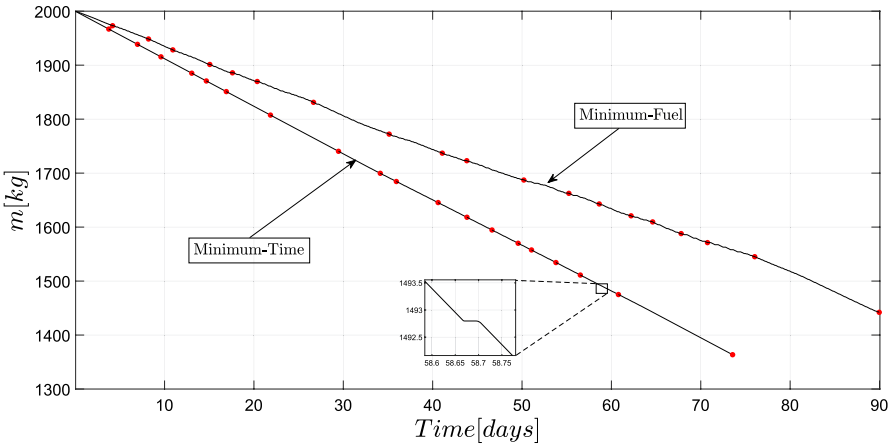

Fig. 10 Minimum-time vs minimum-fuel mass depletion comparison

to the minimum-time case. This comparison underscores the value of applying the Q-law in both scenarios, as it helps evaluate the time-fuel trade-off, which is crucial for assessing mission feasibility and operational constraints during the preliminary design phase.

Finally, the full visiting sequence trajectory is shown in Figs. 11, and 12 respectively for the minimum-time and minimum-fuel cases in Cartesian coordinates. The client orbits and the eclipse phases are intentionally not shown in Fig. 12 to make coast arcs more visible (in red).

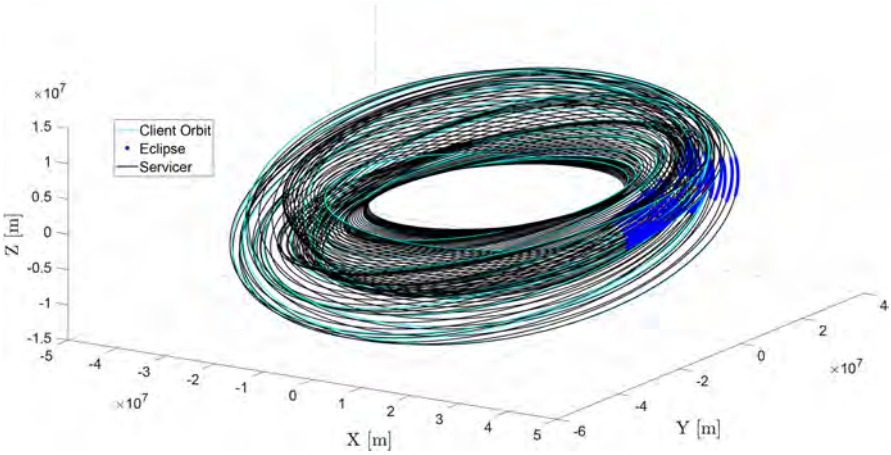

Fig. 11 Optimal sequence trajectory (minimum-time)

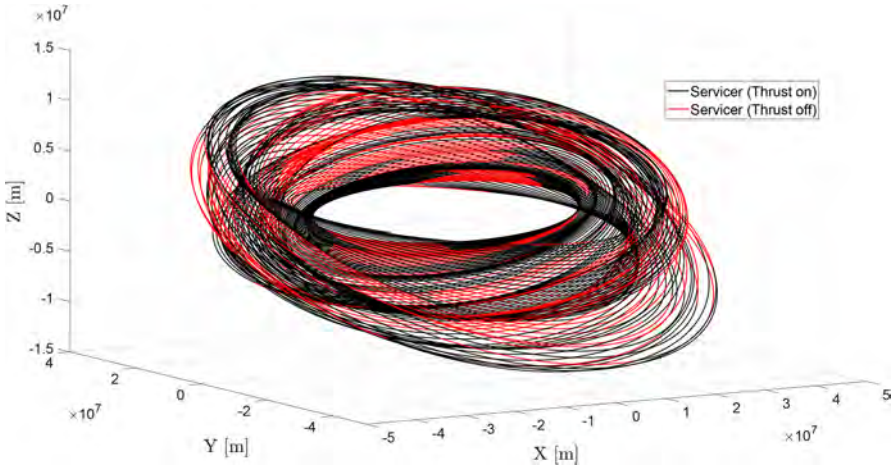

Fig. 12 Optimal sequence trajectory (minimum-fuel)

7.3 Direct Optimization Method Validation

The accuracy of the Q-law was compared with GPOPS-II [43] direct optimization software for both minimum-time and minimum-fuel optimal sequences. The dynamics model implemented for the validation included the J_2 (secular, long and short period terms) and the same eclipse model as presented in Sect. 3. Equinoctial elements propagation was employed in order to avoid singularities and client orbits were propagated by means of Eq. 6. Table 7 reports the GPOPS-II simulation settings.

Each leg of the optimal sequences was compared with GPOPS-II simulations, using the same initial servicer state, global time, and targeted client elements as those used in the Q-law. The first guess was provided by discretizing the Q-law state trajectories and controls into $10 \times N_{rev}$ mesh points where N_{rev} is the number

Table 7 GPOPS-II settings

GPOPS-II Setting	Value
NLP Solver	IPOPT
Linear Solver	ma57
Derivative Type	Central Differences
Collocation Method	RPM-Differentiation
Scales Method	Automatic-bounds
NLP Tolerance	1×10^{-7}
Mesh Method	hp-LiuRao-Legendre
Mesh Tolerance	1×10^{-4}
Max Col. Pts	14
Min Col. Pts	2

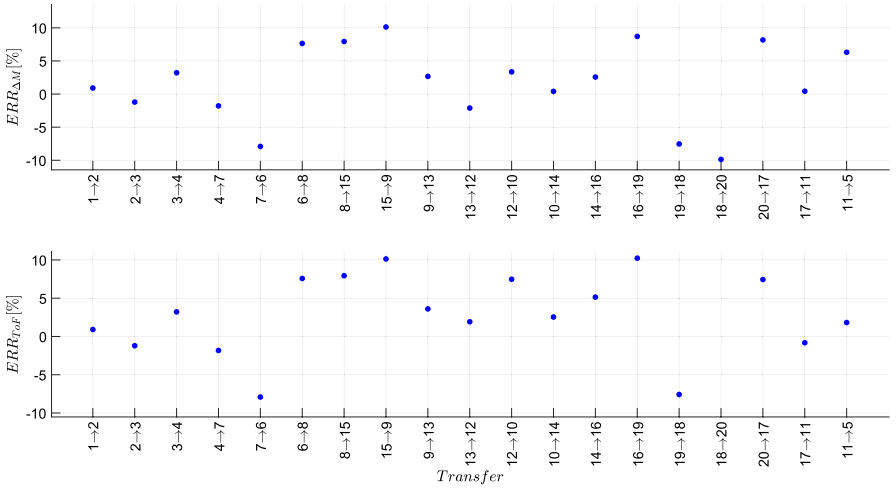

Fig. 13 Minimum-time optimal sequence validation

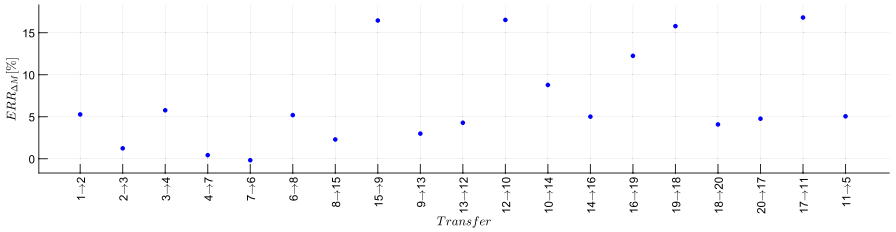

Fig. 14 Minimum-fuel optimal sequence validation

of revolutions of the transfer maneuver. The error in both fuel consumption and time of flight were measured individually for each leg of the optimal sequences. For each leg of the sequence, the initial state and time correspond to those obtained by the GPOPS-II simulations after the convergence to the previous visitation. In the minimum-fuel case, the final time was set as equal to that calculated by the Q-law to assess the coast arc mechanism accuracy. In the minimum-time case the comparison is straightforward and no other considerations are needed. The errors in terms of fuel consumption and time of flight were quantified using Eq. 26.

$$\begin{aligned} ERR_{\Delta m} &= \frac{\Delta m_{QL} - \Delta m_{GP}}{\Delta m_{GP}} \cdot 100 \\ ERR_{ToF} &= \frac{ToF_{QL} - ToF_{GP}}{ToF_{GP}} \cdot 100 \end{aligned} \tag{26}$$

In Eq. 26, the subscripts *QL* and *GP* refer to the values computed by the Q-law and GPOPS-II, respectively. Figures 13 and 14 show the percentage errors per leg for

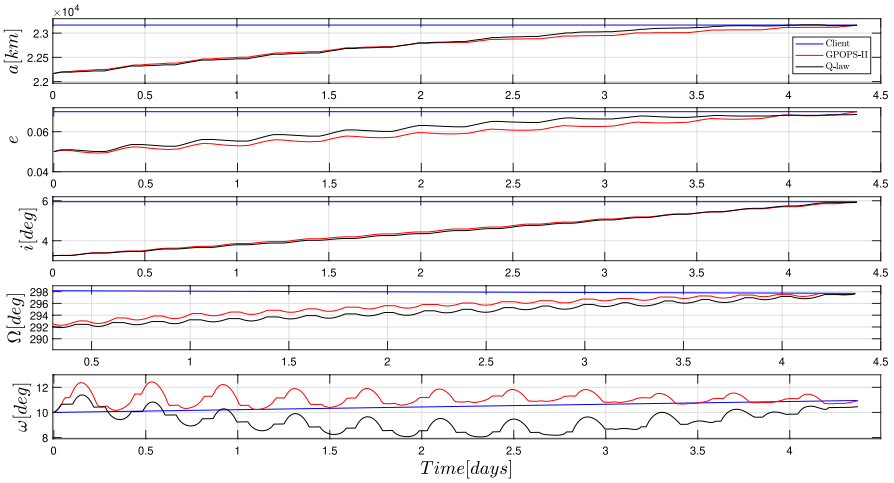

Fig. 15 Keplerian elements history comparison, transfer 1 → 2 (minimum-fuel)

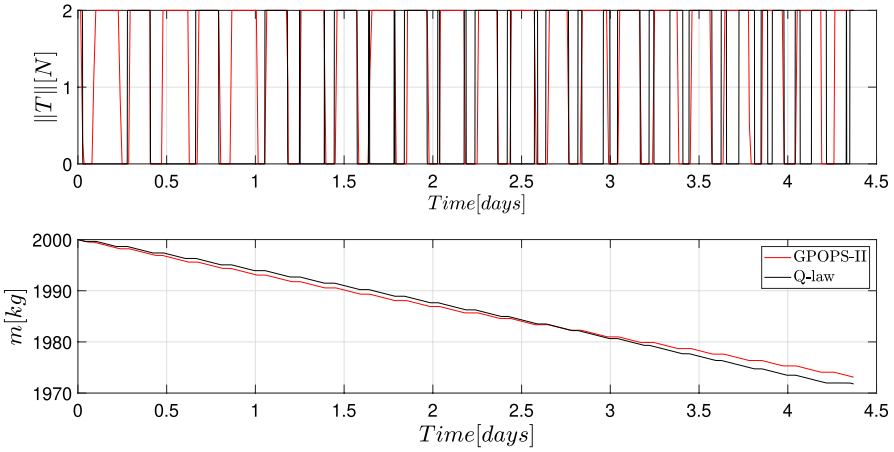

Fig. 16 Thrust norm and mass history comparison, transfer 1 → 2 (minimum-fuel)

both minimum-time and minimum-fuel cases. A more detailed report is provided in Appendix C.

In the minimum-time case, the Q-law estimations per leg of both fuel depletion and time of flight report an absolute maximum error of about 10 % compared to the real optimal values. In the minimum-fuel case, the Q-law fuel depletion estimations show worse performance; however, the percentage error never exceeds 17 %. The fuel depletion and total time of flight estimation errors for the total sequence cost decrease to respectively 3.11 % and 2.81 % in the

minimum-time case and to 7.10 % for the mass depletion in the minimum-fuel case.

Finally, in Figs. 15 and 16 a comparison between GPOPS-II and Q-law results is shown for the transfer $1 \rightarrow 2$ in terms of Keplerian elements, thrust norm, and mass history, respectively (minimum-fuel case). It is evident how the Q-law provides a good first guess for the direct optimization method; important differences in thrust switching times are visible, which nevertheless cause minor fuel savings.

8 Conclusions

A new method has been developed, building upon the approach previously proposed in [4], to address multi-target optimal path optimization problems in the context of low-thrust propulsion. The algorithm incorporates the main time-dependent factors, including perturbations (secular J_2 effects and propulsion constraint due to eclipse) as well as servicer fuel mass depletion.

The overall problem is decomposed into two parts: the functional problem and the combinatorial problem. The functional problem is solved for all possible transfers between the satellites of a dataset and for discrete values of initial mass and departure time ranging in pre-defined intervals. The cost in terms of both fuel and time of flight is assessed by a Q-law-based distance metric for both minimum-time and minimum-fuel problems. This procedure provides two four-variable arrays. Bilinear interpolation is then applied to estimate the costs for continuous values of initial mass and departure times. The problem is thus reduced to a pure combinatorial problem where generic constraints and objective function formulations can be considered.

The methodology is demonstrated on a benchmark problem where a servicer spacecraft must visit multiple targets once and only once. In this work, a genetic algorithm, simulated annealing, and particle swarms are employed to solve the combinatorial problem and compared in terms of accuracy and computational times. Each of them is run multiple times to assure the convergence to the global optimum. For all simulations, the optimal sequence is found in less than five minutes. The accuracy of the proposed approach is assessed by a direct optimization method. Small errors in terms of total fuel mass expenditure and total time of flight are reported.

Key features of the proposed approach are the computational efficiency and flexibility. The method can be applied to solve a variety of mission scenarios by appropriately defining the objective function and constraints of the combinatorial

problem. For instance, it can address on-orbit refueling problems, where the goal is to maximize the number of clients refueled within the constraints of the servicer's maximum available fuel, or multi-platform open tour problems, where multiple servicers are tasked with visiting all clients in a dataset exactly once while minimizing the total fuel consumption. Limitations of the proposed approach may arise in highly perturbative environments, such as low Earth orbit, where accelerations due to the J_2 effect can exceed the servicer's available control acceleration. Under these conditions, the Q-law may lead to reduced solution accuracy.

Overall, the results indicate that the proposed algorithm would serve as a valuable tool to solve low-thrust multi-target path optimization problems.

Appendix A Q-law Analytic Functions

The following expressions for constructing the Lyapunov function in the Q-law derivation are presented in [21]

$$P = e^{k\left(1-\frac{r_p}{r_{p\min}}\right)}$$

$$S_i = \begin{cases} \left[1+\left(\frac{X_i - X_{T,i}}{mX_{T,i}}\right)^n\right]^{1/r} & i = 1 \\ 1 & \text{otherwise} \end{cases}$$

$$\max_\theta(\dot{a}) = 2u\sqrt{\frac{a^3(1+e)}{\mu(1-e)}}$$

$$\max_\theta(\dot{e}) = \frac{2pu}{h}$$

$$\max_\theta(\dot{i}) = \frac{pu}{h\left(\sqrt{1-e^2\sin^2(\omega)}-e|\cos(\omega)|\right)}$$

$$\max_\theta(\dot{\Omega}) = \frac{pu}{h\sin(i)\left(\sqrt{1-e^2\cos^2(\omega)}-e|\sin(\omega)|\right)}$$

$$\max_\theta(\dot{\omega}) = \frac{\max_\theta\left(\dot{\omega}_{\text{ip}}\right)+b\max_\theta\left(\dot{\omega}_{\text{op}}\right)}{(1+b)}$$

$$\max_\theta(\dot{\omega}_{\text{ip}}) = \frac{u\sqrt{p^2\cos^2(\theta_{xx})+(p+r_{xx})^2\left(1-\cos^2(\theta_{xx})\right)}}{eh}$$

$$\max_\theta(\dot{\omega}_{\text{op}}) = \frac{pu|\cos(i)|}{h\sin(i)\left(\sqrt{1-e^2\cos^2(\omega)}-e|\sin(\omega)|\right)}$$

$$\cos\theta_{xx} = \left[\frac{1-e^2}{2e^3}+\sqrt{\frac{1}{4}\left(\frac{1-e^2}{e^3}\right)^2+\frac{1}{27}}\right]^{\frac{1}{3}} - \left[-\frac{1-e^2}{2e^3}+\sqrt{\frac{1}{4}\left(\frac{1-e^2}{e^3}\right)^2+\frac{1}{27}}\right]^{\frac{1}{3}} - \frac{1}{e}$$

$$r_{xx} = \frac{p}{1+e\cos(\theta_{xx})}$$

where $k = 100$, $m = 3$, $n = 2$, $r = 2$, $b = 0.01$, $r_{p\min} = 6578$ km, $r_p = a(1-e)$ is the periapsis distance, $u(t) = T(t)/m(t)$ is the instantaneous control acceleration norm ($T(t)$ being the thrust magnitude), μ is the gravitational constant, $p = a(1-e^2)$, and $h = \sqrt{\mu p}$.

Appendix B Eclipse Constraint Model

Denoting with $t_{JD}(t)$ the Julian date corresponding to time t, $\mathbf{r}_S(t_{JD})$ the Sun's position with respect to the ECI frame, $\mathbf{r}_{sc}(\mathbf{X}(t))$ the spacecraft position with respect to the ECI frame as a funciton of the Keplerian state $\mathbf{X}(t) = [a(t), e(t), i(t), \Omega(t), \omega(t), \theta(t)]^\intercal$, R_e as

Table 8 Minimum-time optimal sequence validation results

Transfer	Δm_{QL} [kg]	Δm_{GP} [kg]	$ERR_{\Delta m}$ [%]	ToF_{QL} [days]	ToF_{GP} [days]	ERR_{ToF} [%]
1 → 2	33.22	32.92	0.907	3.770	3.736	0.907
2 → 3	28.22	28.57	−1.216	3.203	3.242	−1.216
3 → 4	22.95	22.24	3.209	2.605	2.524	3.209
4 → 7	30.47	31.03	−1.789	3.458	3.523	−1.833
7 → 6	14.55	15.80	−7.917	1.651	1.793	−7.917
6 → 8	19.68	18.28	7.640	2.234	2.076	7.572
8 → 15	43.32	40.13	7.934	4.917	4.555	7.934
15 → 9	66.81	60.66	10.12	7.583	6.885	10.13
9 → 13	41.34	40.27	2.662	4.740	4.575	3.598
13 → 12	13.98	14.29	−2.121	1.660	1.629	1.917
12 → 10	39.77	38.48	3.347	4.763	4.432	7.466
10 → 14	27.30	27.19	0.403	3.247	3.167	2.536
14 → 16	23.60	23.01	2.562	2.806	2.669	5.132
16 → 19	24.49	22.54	8.705	2.916	2.645	10.22
19 → 18	12.47	13.49	−7.542	1.503	1.627	−7.588
18 → 20	23.28	25.84	−9.878	2.729	3.081	−11.39
20 → 17	23.20	21.45	8.168	2.734	2.545	7.440
17 → 11	36.08	35.92	0.422	4.260	4.295	−0.827
11 → 5	110.5	104.0	6.302	12.67	12.44	1.817
Total Sequence	635.4	616.2	3.114	73.46	71.45	2.806

Table 9 Minimum-fuel optimal sequence validation results

Transfer	Δm_{QL} [kg]	Δm_{GP} [kg]	$ERR_{\Delta m}$ [%]	$ToF_{QL} = ToF_{GP}$ [days]
1 → 2	28.21	26.80	5.278	4.371
2 → 3	23.47	23.19	1.241	3.719
3 → 4	20.99	19.84	5.768	3.081
4 → 7	27.03	26.91	0.428	4.100
7 → 6	15.11	15.14	−0.173	2.263
6 → 8	17.05	16.21	5.193	3.068
8 → 15	38.21	37.36	2.295	6.305
15 → 9	60.31	51.79	16.45	9.247
9 → 13	35.60	34.56	2.992	6.389
13 → 12	14.77	14.16	4.283	2.623
12 → 10	36.31	31.16	16.52	6.785
10 → 14	25.07	23.05	8.784	5.118
14 → 16	20.13	19.17	5.009	3.887
16 → 19	22.37	19.93	12.24	3.739
19 → 18	11.37	9.827	15.78	3.113
18 → 20	22.58	21.69	4.083	3.546
20 → 17	17.79	16.98	4.766	4.190
17 → 11	28.59	24.47	16.81	5.687
11 → 5	104.1	99.12	5.054	15.17
Total Sequence	569.2	531.4	7.103	96.41

the mean Earth radius, and R_S as the Sun mean radius, the eclipse factor can be computed as [44]

$$\mathbf{r}_{S/sc} = \mathbf{r}_S - \mathbf{r}_{sc}$$

$$a_{SR} = \arcsin\left(\frac{R_S}{r_{S/sc}}\right)$$

$$a_{BR} = \arcsin\left(\frac{R_e}{r_{sc}}\right)$$

$$a_D = \arccos\left(\frac{\mathbf{r}_{sc}^T \mathbf{r}_{S/sc}}{r_{sc} r_{S/sc}}\right)$$

$$w_{ecl}(\mathbf{X}(t), t_{JD}) = \frac{1}{1 + e^{-c_s[a_D - c_t(a_{SR} + a_{BR})]}}$$

where the coefficients assume the values $C_s = 298.78$ and $C_t = 1$. w_{ecl} is a continuous function bounded between 0 and 1; $w_{ecl} = 0$ if the satellite is in eclipse ($a_{SR} + a_{BR} > a_D$), $0 < w_{ecl} < 1$ in penumbra and $w_{ecl} = 1$ otherwise. In this work, the eclipse caused by Earth's shadow is considered, and the Sun's ephemeris model, as described in [45], is adopted.

Appendix C GPOPS-II Validation Details

Tables 8 and 9 report the fuel consumption and time of flight as computed by the Q-law and GPOPS-II validation for each leg of the optimal sequence both in the minimum-time and minimum-fuel cases.

Acknowledgements The participation of Dr. Jennifer Hudson and Dr. Bhattacharjee Shambo was partially supported by the U.S. Defense Innovation Unit. The participation of Riccardo Apa was supported by the project NODES which has received funding from the MUR - M4C2 1.5 of PNRR funded by the European Union - NextGenerationEU (Grant agreement no. ECS00000036), and the participation of Dr. Marcello Romano was partially supported by a grant of Compagnia di San Paolo.

Funding Open access funding provided by Politecnico di Torino within the CRUI-CARE Agreement.

Data availability No external data were used in this study, and no data repository has been created.

Declarations

Conflict of interest The author declares that there exists no competing financial interest or personal relationships that could have appeared to influence the work reported in this paper.

References

1. ISAM Interagency Working Group: In-Space Servicing, Assembly, and Manufacturing (ISAM) National Strategy. National Science and Technology Council, Washington DC (2022)
2. Zhu, X., Zhang, C., Sun, R., Chen, J., Wan, X.: Orbit determination for fuel station in multiple SSO spacecraft refueling considering the J2 perturbation. Aerosp. Sci. Technol. **105**, 105994 (2020)
3. Schneider, J.: The time-dependent traveling salesman problem. Phys. A Statis. Mech. Appl. **314**(1–4), 151–155 (2002). https://doi.org/10.1016/S0378-4371(02)01078-6
4. Cerf, M.: Multiple Space Debris Collecting Mission: Optimal Mission Planning. J. Optimiz. Theory Appl. **167**(1), 195–218 (2015). https://doi.org/10.1007/s10957-015-0705-0
5. Madakat, D., Morio, J., Vanderpooten, D.: Biobjective planning of an active debris removal mission. Acta Astronautica **84**, 182–188 (2013) https://doi.org/10.1016/j.actaastro.2012.10.038
6. Bourjolly, J., Gurtuna, O., Lyngvi, A.: On-orbit servicing: a time-dependent, moving-target traveling salesman problem. Int. Transac. Oper. Res. **13**(5), 461–481 (2006). https://doi.org/10.1111/j.1475-3995.2006.00558.x
7. Kanazaki, M., Yamada, Y., Nakamiya, M.: Trajectory optimization of a satellite for multiple active space debris removal based on a method for the traveling serviceman problem. In: 2017 21st Asia Pacific Symposium on Intelligent and Evolutionary Systems (IES), pp. 61–66 (2017). https://doi.org/10.1109/IESYS.2017.8233562
8. Cerf, M.: Multiple Space Debris Collecting Mission-Debris Selection and Trajectory Optimization. J. Optimiz. Theory Appl. **156**(3), 761–796 (2013). https://doi.org/10.1007/s10957-012-0130-6

9. Verstraete, A.W., Anderson, D., St. Louis, N.M., Hudson, J.: Geosynchronous Earth Orbit Robotic Servicer Mission Design. J. Spacecr. Rockets **55**(6), 1444–1452 (2018) https://doi.org/10.2514/1.A33945
10. Hudson, J.S., Kolosa, D.: Versatile On-Orbit Servicing Mission Design in Geosynchronous Earth Orbit. J. Spacecr. Rockets **57**(4), 844–850 (2020). https://doi.org/10.2514/1.A34701
11. Wijayatunga, M.C., Armellin, R., Holt, H., Pirovano, L., Lidtke, A.A.: Design and guidance of a multi-active debris removal mission. Astrodynamics **7**(4), 383–399 (2023). https://doi.org/10.1007/s42064-023-0159-3
12. Jorgensen, M.K., Sharf, I.: Optimal planning for a multiple space debris removal mission using high-accuracy low-thrust transfers. Acta Astronautica **172**, 56–69 (2020) https://doi.org/10.1016/j.actaastro.2020.03.031
13. Gatto, G., Casalino, L.: Fast Evaluation and Optimization of Low-Thrust Transfers to Multiple Targets. J. Guid. Control Dyn. **38**(8), 1525–1530 (2015). https://doi.org/10.2514/1.G001116
14. Li, H., Chen, S., Baoyin, H.: J2-perturbed multitarget rendezvous optimization with low thrust. J. Guid. Control Dyn. **41**(3), 802–808 (2018)
15. Narayanaswamy, S., Wu, B., Ludivig, P., Soboczenski, F., Venkataramani, K., Damaren, C.J.: Low-thrust rendezvous trajectory generation for multi-target active space debris removal using the RQ-Law. Adv. Space Res. **71**(10), 4276–4287 (2023). https://doi.org/10.1016/j.asr.2022.12.049
16. Zuiani, F., Vasile, M.: Preliminary Design of Debris Removal Missions by Means of Simplified Models for Low-Thrust, Many-Revolution Transfers. Int. J. Aerospace Eng. **2012**, 1–22 (2012) https://doi.org/10.1155/2012/836250
17. Sarton Du Jonchay, T., Chen, H., Isaji, M., Shimane, Y., Ho, K.: On-Orbit Servicing Optimization Framework with High- and Low-Thrust Propulsion Tradeoff. J. Spacecr. Rockets **59**(1), 33–48 (2022) https://doi.org/10.2514/1.A35094
18. Lee, D., Ahn, J.: Optimal Multitarget Rendezvous Using Hybrid Propulsion System. J. Spacecr. Rockets **60**(2), 689–698 (2023). https://doi.org/10.2514/1.A35540
19. Varga, G.I., Pérez, J.S.: Many-revolution low-thrust orbit transfer computation using equinoctial Q-law including J2 and eclipse effects. In: 6th International Conference on Astrodynamics Tools and Techniques, vol. 1, pp. 29–42 (2016). Darmstatd Germany
20. Apa, R., Kaminer, I., Hudson, J., Romano, M.: Optimal low-thrust orbital transfer for servicing multiple satellites in elliptical orbits. Acta Astronautica **228**, 686–699 (2025) https://doi.org/10.1016/j.actaastro.2024.12.030
21. Petropoulos, A.E.: Simple control laws for low-thrust orbit transfers. Adv. Astronaut. Sci. **116**, 2031–2047 (2003)
22. Davendra, D.: Traveling Salesman Problem. IntechOpen, Rijeka (2010). https://doi.org/10.5772/547
23. Conway, B.A. (ed.): Spacecraft Trajectory Optimization. Cambridge University Press, Cambridge (2010). https://doi.org/10.1017/CBO9780511778025
24. Topputo, F., Zhang, C.: Survey of Direct Transcription for Low-Thrust Space Trajectory Optimization with Applications. Abstr. Appl. Anal. **2014**, 1–15 (2014) https://doi.org/10.1155/2014/851720
25. Violina, S.: Analysis of brute force and branch & bound algorithms to solve the traveling salesperson problem (TSP). Turk. J. Comput. Mathemat. Educat. **12**(8), 1226–1229 (2021)
26. Jünger, M., Reinelt, G., Rinaldi, G.: The traveling salesman problem. In: Network Models. Handbooks in Operations Research and Management Science, vol. 7, pp. 225–330. Elsevier, Amsterdam, Netherlands (1995). https://doi.org/10.1016/S0927-0507(05)80121-5
27. Winter Althaus, G. (ed.): Genetic Algorithms in Engineering and Computer Science. Wiley, Chichester (1995)
28. Rutenbar, R.A.: Simulated annealing algorithms: an overview. IEEE Circuits and Devices Magazine **5**(1), 19–26 (1989). https://doi.org/10.1109/101.17235
29. Kennedy, J., Eberhart, R.: Particle swarm optimization. In: Proceedings of ICNN'95 - International Conference on Neural Networks, vol. 4, pp. 1942–19484 (1995). https://doi.org/10.1109/ICNN.1995.488968
30. Edelbaum, T.N.: Optimum low-thrust rendezvous and station keeping. AIAA J. **2**(7), 1196–1201 (1964). https://doi.org/10.2514/3.2521
31. Di Carlo, M., Romero Martin, J.M., Vasile, M.: Automatic trajectory planning for low-thrust active removal mission in low-earth orbit. Adv. Space Res. **59**(5), 1234–1258 (2017). https://doi.org/10.1016/j.asr.2016.11.033

32. Curtis, H.D.: Introduction to orbital perturbations. In: Curtis, H.D. (ed.) Orbital Mechanics for Engineering Students, 3rd edn., pp. 651–720. Butterworth-Heinemann, Boston (2014). https://doi.org/10.1016/B978-0-08-097747-8.00012-8
33. Holt, H.J.: Trajectory design using Lyapunov control laws and reinforcement learning. PhD thesis, University of Surrey (2023). Section 2.1
34. Kluever, C.A.: Using Edelbaum's method to compute low-thrust transfers with earth-shadow eclipses. J. Guid. Control Dyn. **34**(1), 300–303 (2011). https://doi.org/10.2514/1.51024
35. Schaub, H., Junkins, J.L.: Analytical Mechanics Of Space Systems. American Institute of Aeronautics and Astronautics, Reston ,VA (2003). https://doi.org/10.2514/4.861550
36. Lawden, D.F.: Optimal Trajectories for Space Navigation. Butterworths, London (1963)
37. Prussing, J.E.: Primer vector theory and applications. In: Conway, B.A. (ed.) Spacecraft Trajectory Optimization, 1st edn., pp. 16–36. Cambridge University Press, Cambridge, UK (2010). https://doi.org/10.1017/CBO9780511778025.003
38. Petropoulos, A.: Low-Thrust Orbit Transfers Using Candidate Lyapunov Functions with a Mechanism for Coasting. In: AIAA/AAS Astrodynamics Specialist Conference And Exhibit. American Institute of Aeronautics and Astronautics, Providence, Rhode Island (2004). https://doi.org/10.2514/6.2004-5089
39. Shannon, J.L., Ozimek, M.T., Atchison, J.A., Christine, M.: Q-law aided direct trajectory optimization for the high-fidelity, many-revolution low-thrust orbit transfer problem. Adv. Astronautic. Sci. **168**, 781–800 (2019)
40. Press, W.H., Teukolsky, S.A., Vetterling, W.T., Flannery, B.P.: Numerical Recipes in C: The Art of Scientific Computing, 2nd edn., pp. 91–139. Cambridge University Press, Cambridge, UK (1995). Chap. 3
41. MathWorks: MATLAB version: 23.2 (R2023b). The MathWorks Inc., Natick, Massachusetts (2023). https://www.mathworks.com
42. Izzo, D., Getzner, I., Hennes, D., Simões, L.F.: Evolving Solutions to TSP Variants for Active Space Debris Removal. In: Proceedings of the 2015 Annual Conference on Genetic and Evolutionary Computation, pp. 1207–1214. ACM, Madrid Spain (2015). https://doi.org/10.1145/2739480.2754727
43. Patterson, M.A., Rao, A.V.: GPOPS-II: A MATLAB software for solving multiple-phase optimal control problems using hp-adaptive gaussian quadrature collocation methods and sparse nonlinear programming. ACM Transac. Mathemat. Softw. **41**(1), 1–37 (2014). https://doi.org/10.1145/2558904
44. Aziz, J., Scheeres, D., Parker, J., Englander, J.: A smoothed eclipse model for solar electric propulsion trajectory optimization. Transac. Japan Soc. Aeronaut. Space Sci. Aerospace Technol. Japan **17**(2), 181–188 (2019). https://doi.org/10.2322/tastj.17.181
45. Montenbruck, O., Gill, E., Lutze, F.: Satellite Orbits: Models, Methods, and Applications. Appl. Mech. Rev. **55**(2), 27–28 (2002). https://doi.org/10.1115/1.1451162

Authors and Affiliations

Riccardo Apa[1] · Shambo Bhattacharjee[2] · Jennifer Hudson[2] · Marcello Romano[3]

✉ Riccardo Apa
riccardo.apa@polito.it

Shambo Bhattacharjee
shambo.bhattacharjee.in@nps.edu

Jennifer Hudson
jennifer.hudson@nps.edu

Marcello Romano
marcello.romano@tum.de

[1] Mechanical and Aerospace Eng., Politecnico di Torino, Corso Duca degli Abruzzi 24, 10129 Torino, Italy

[2] Mechanical and Aerospace Eng., Naval Postgraduate School, 1 University Cir., 93943 Monterey, CA, USA

[3] Chair of Astrodynamics, Technical University of Munich (TUM), Lise-Meitner-Strasse 8, 85521 Ottobrunn, Germany